

Non-Oberbeck-Boussinesq effects in strongly turbulent Rayleigh-Bénard convection

By Guenter Ahlers¹, Eric Brown¹, Francisco Fontenele Araujo²,
Denis Funfschilling¹, Siegfried Grossmann³, and Detlef Lohse²

¹Department of Physics and iQCD, University of California, Santa Barbara, CA 93106,

²Department of Science and Technology and J.M. Burgers Center for Fluid Dynamics,
University of Twente, P.O. Box 217, 7500 AE Enschede, The Netherlands,

³Fachbereich Physik der Philipps-Universität, Renthof 6, D-35032 Marburg, Germany

(Received 12 April 2006)

Non-Oberbeck-Boussinesq (NOB) effects on the Nusselt number Nu and Reynolds number Re in strongly turbulent Rayleigh-Bénard convection in liquids were investigated both experimentally and theoretically. In the experiment, the heat current, the temperature difference, and the temperature at the horizontal mid-plane were measured. Three cells of different heights L , all filled with water and all with aspect ratio Γ close to 1, were used. For each L , about 1.5 decades in Ra were covered, together spanning the range $10^8 \leq Ra \leq 10^{11}$. For the largest temperature difference between the bottom and top plates of $\Delta = 40\text{K}$ the kinematic viscosity and the thermal expansion coefficient, due to their temperature dependence, varied by more than a factor of two. The Oberbeck-Boussinesq (OB) approximation of temperature independent material parameters thus was no longer valid. The ratio χ of the temperature drops across the bottom and top thermal boundary layers became as small as $\chi = 0.83$, as compared to the ratio $\chi = 1$ in the OB case. Nevertheless, the Nusselt number Nu was found to be only slightly smaller (at most 1.4%) than in the next larger cell with the same Rayleigh number, where the material parameters were still nearly height-independent. The Reynolds numbers in the OB and NOB case agreed with each other within the experimental resolution of about 2%, showing that NOB effects for this parameter were small as well. Thus Nu and Re are rather insensitive against even significant deviations from OB conditions. Theoretically, we first account for the robustness of Nu with respect to NOB corrections: the NOB effects in the top boundary layer cancel those which arise in the bottom boundary layer as long as they are linear in the temperature difference Δ . The net effects on Nu are proportional to Δ^2 and thus increase only slowly and still remain minor despite drastic material parameter changes. We then extend the Prandtl-Blasius boundary-layer theory to NOB Rayleigh-Bénard flow with temperature dependent viscosity and thermal diffusivity. This allows the calculation of the shift of the bulk temperature, the temperature drops across the boundary layers, and the ratio χ without introducing any fitting parameter. The calculated quantities are in very good agreement with experiment. When in addition we use the experimental finding that for water the sum of the top and bottom thermal boundary-layer widths (based on the slopes of the temperature profiles at the plates) remains unchanged under NOB effects within experimental resolution, the theory also gives the measured small Nusselt-number reduction for the NOB case. In addition, it predicts an increase by about 0.5% of the Reynolds number, which is also consistent with the experimental data. By theoretically studying hypothetical liquids with only one of the material parameters being temperature dependent, we shed further light on the origin of NOB corrections in water: While the NOB deviation of χ from its OB value $\chi = 1$ mainly originates from the temperature dependence of the viscosity, the NOB

correction of the Nusselt number primarily originates from the temperature dependence of the thermal diffusivity. Finally, we give the predictions from our theory for the NOB corrections if glycerol is used as operating liquid.

1. Introduction

Controlled experiments on Rayleigh-Bénard (RB) convection are normally done with relatively small temperature differences Δ between the top and the bottom plate, so that the Oberbeck-Boussinesq (OB) approximation can be used. That approximation assumes that the material properties such as the kinematic viscosity ν , the thermal diffusivity κ , the heat conductivity Λ , the isobaric specific heat capacity c_p , and the isobaric thermal expansion coefficient β can be considered to be temperature independent and thus to have constant values all over the cell (Oberbeck (1879); Boussinesq (1903)). However, in order to achieve large Rayleigh numbers Ra , one would like to make Δ as large as possible. One of the relatively well analyzed effects due to deviations from OB conditions is that the temperature drops across the top and the bottom thermal boundary layers (Wu & Libchaber (1991); Zhang *et al.* (1997)) become different, i.e., an asymmetry with respect to the mid-plane of the cell shows up. However, it is unclear what the associated NOB effects on the Nusselt number Nu and the Reynolds number Re are. Nonetheless, it is often argued in very general terms that NOB effects are responsible for some measured large Ra peculiarities in Nu or Re . The lack of our understanding of possible NOB effects at large Ra on Nu and Re measurements are the more unsatisfactory, as it is this large Ra regime where the crossover to an ultimate scaling regime $Nu \sim Ra^{1/2}$ is expected (Kraichnan (1962)). In helium gas beyond $Ra \approx 10^{11}$ Chavanne *et al.* (1997, 2001) find a steeper increase of the logarithmic slope of the $Nu(Ra)$ curve as compared to Niemela *et al.* (2000, 2001) and associate this finding with the ultimate Kraichnan regime. However, there is a major controversy on whether these and other large Ra data are “contaminated” by NOB effects or not (Chavanne *et al.* (1997, 2001); Roche *et al.* (2001, 2002); Niemela *et al.* (2000, 2001); Niemela & Sreenivasan (2003); Ashkenazi & Steinberg (1999)).

The aim of this paper is to first present systematic measurements of NOB effects on the Nusselt number Nu , the Reynolds number Re , and on the center temperature T_c of the cell, and then to theoretically understand these NOB effects. We do so by extending the Prandtl-Blasius boundary layer theory to the case of temperature dependent viscosity and thermal diffusivity and apply it to NOB Rayleigh-Bénard flow. Our results hold for liquids, whose specific heat capacity c_p and density ρ except for buoyancy are temperature independent in sufficiently good approximation, and if the flow is incompressible.

For small Ra close to the transition to convection and pattern formation NOB effects were treated theoretically by various authors, and most systematically by Busse (1967). They were examined experimentally by Hoard *et al.* (1970); Ahlers (1980); Walden & Ahlers (1981); Ciliberto *et al.* (1988); Bodenschatz *et al.* (1991); Pampaloni *et al.* (1992); and reviewed by Bodenschatz *et al.* (2000).

The outline of the paper is as follows: In Sect. 2 we introduce our notations and define quantitative measures of NOB effects. These include different thicknesses of the thermal boundary layers (BL) as well as different temperature drops at the bottom and the top plates. In section 3 we present our experimental results for the various measures of NOB effects, in particular for Nu and Re . We find robustness of Nu and Re towards NOB effects which we try to rationalize in section 4. In section 5 we briefly review the model

of Wu & Libchaber (1991) and Zhang *et al.* (1997), who analyzed NOB effects on RB flow with cryogenic helium gas and with glycerin, both experimentally and theoretically. We compare the predictions of their model with our data for water. Although they correctly predict the robustness of Nu with respect to NOB effects and even account for the very small Nu decrease for the NOB case, it turns out that one of the basic assumptions of the model is not fulfilled. In Section 6 we apply an extended Prandtl-Blasius boundary layer theory to the NOB Rayleigh-Bénard flow, giving excellent agreement for the center temperature, the Nusselt number, and the Reynolds number with the measured data. Section 7 contains the conclusions.

2. Characterization of non-Oberbeck-Boussinesq effects

2.1. Control parameters

What fluid properties should be used to define the non-dimensional numbers of non-Oberbeck-Boussinesq Rayleigh-Bénard flow? Since the commonly used control parameters are the temperatures T_b and T_t at the bottom and top plates, the immediate choice of a reference temperature to characterize the typical material properties is the mean temperature $T_m = (T_t + T_b)/2$. The overall temperature drop is $\Delta = T_b - T_t$. The corresponding definition of the parameters describing the thermal convection is the Rayleigh number

$$Ra_m = \frac{\beta_m g \Delta L^3}{\nu_m \kappa_m} \equiv Ra, \quad (2.1)$$

the Prandtl number

$$Pr_m = \nu_m / \kappa_m \equiv Pr, \quad (2.2)$$

and, as a response of the system, the Reynolds number of the resulting large-scale circulation (the “wind”)

$$Re_m = \frac{UL}{\nu_m} \equiv Re. \quad (2.3)$$

Here U is the mean velocity of the large scale wind in the bulk of the fluid. We assume that there is only one such velocity scale, or, to be more precise, that the velocity of the wind is the same close to the top and close to the bottom of the cell. The label m indicates that the material parameters are those at the mean temperature T_m . In the following we shall skip the label m of Ra , Pr , Re , and later also of the Nusselt number Nu . Whenever these nonlabelled dimensionless parameters are used, the respective material properties are meant as those at the mean temperature T_m of the external control temperatures. The actual time averaged temperature in the bulk is called T_c . It is different from T_m due to NOB effects, $T_c \neq T_m$.

The notation used in this paper is shown in figure 1. The fluid properties such as ν , κ , and β carry the same index as the corresponding temperature at which they are considered, e.g., $\nu_t = \nu(T_t)$ for the kinematic viscosity at the top plate, and so on.

2.2. Temperature profile

Wu & Libchaber (1991) have shown that for NOB thermal convection in cryogenic helium the temperature drop across the top BL Δ_t is smaller than the temperature drop across the bottom BL Δ_b . In contrast, for NOB thermal convection in glycerol Zhang *et al.* (1997) showed that the opposite is the case, i.e., $\Delta_t > \Delta_b$. In general, the ratio of the

temperature drops is described by the parameter†

$$\chi = \chi_\Delta = \Delta_b/\Delta_t. \quad (2.4)$$

Just as in large Ra Rayleigh-Bénard flow under OB conditions, we have no indication that for the time averaged profile there is a temperature drop across the bulk (center) of the RB cell, and therefore we assume that the total temperature difference between the cold top plate temperature T_t and the hot bottom plate temperature $T_b = T_t + \Delta$ consists only of the temperature drops across the thermal boundary layers,

$$\Delta = \Delta_t + \Delta_b. \quad (2.5)$$

The time averaged temperature in the center of the cell then is $T_c = T_t + \Delta_t = T_b - \Delta_b$. It deviates from T_m and expresses the response of the system to the NOB effects, while T_m is just the arithmetic mean of the external control parameters. Depending on the fluid, T_c may be larger or smaller than T_m .

Equations (2.4) and (2.5) can be solved for the temperature drops Δ_b and Δ_t across the bottom and top thermal BLs,

$$\Delta_b = \frac{\chi}{1 + \chi} \Delta, \quad (2.6)$$

$$\Delta_t = \frac{1}{1 + \chi} \Delta. \quad (2.7)$$

The temperature profile in the container is sketched in figure 1. In section 6 it will be *calculated* within an extended Prandtl-Blasius boundary layer theory.

2.3. Heat flux

The heat flux can be evaluated from the local heat-conservation equation

$$\rho c_p (\partial_t \theta + u_i \partial_i \theta) = \partial_i (\Lambda \partial_i \theta), \quad (2.8)$$

where θ is the temperature deviation from a convenient reference temperature, e.g. T_m . $\partial_i \dots$ means $\partial \dots / \partial x_i$, $i = x, y, z$ are the three coordinates, and summation over repeated equal indices is assumed. By starting from Eq. (2.8) we have already assumed that the variation of the entropy per mass s with pressure p to a good approximation does not contribute, more precisely that $|\frac{dT}{dz}| \gg |\frac{T}{c_p} \left(\frac{\partial s}{\partial p} \right)_T \frac{dp}{dz}|$. Using $\frac{dp}{dz} = -\rho g$, the right hand side of this inequality can be rewritten as $\rho g (\partial T / \partial p)_s \equiv a_g$. Thus we assume that a_g , the adiabatic temperature change with pressure, is much smaller than the applied temperature gradient Δ/L (Furukawa & Onuki (2002); Gitterman (1978); Landau & Lifshitz (1987)). Indeed, for our experiment with water described in Sect. 3 we typically have $a_g L / \Delta \approx 10^{-6}$ for this so called Schwarzschild parameter, i.e., it is negligibly small. Note that for gases close to the critical point the Schwarzschild correction in general cannot be neglected (Gitterman & Steinberg (1971); Gitterman (1978); Ashkenazi & Steinberg (1999); Kogan & Meyer (2001); Furukawa & Onuki (2002)).

We area and time average $\langle \dots \rangle_A$ equation (2.8). The label A indicates planes $z = \text{constant}$, parallel to the top and bottom plates of the container. In addition, we assume that plane averaged products of the type $\langle \rho c_p \partial_z (u_z \theta) \rangle_A$ or $\langle \Lambda \partial_z \theta \rangle_A$ can be approximated by their respective factorizations $\langle \rho c_p \rangle_A \langle \partial_z (u_z \theta) \rangle_A$ and $\langle \Lambda \rangle_A \partial_z \langle \theta \rangle_A$. We then obtain

$$\partial_z [\langle \rho c_p \rangle_A \langle u_z \theta \rangle_A - \Lambda(z) \partial_z \langle \theta \rangle_A] = \langle u_z \theta \rangle_A \partial_z \langle \rho c_p \rangle_A \approx 0. \quad (2.9)$$

In the second (approximate) equality, \approx , we have used the fact that for liquids the mass

† Note that the parameter x of Wu & Libchaber (1991) is $x = \chi^{-1}$.

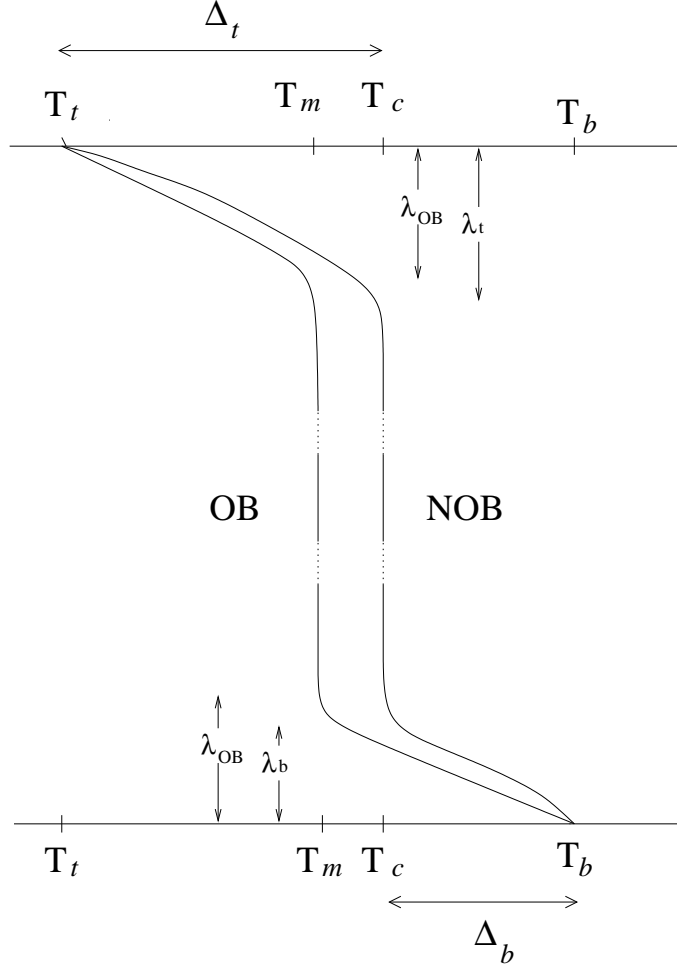


FIGURE 1. Sketch of temperature profile details: The time averaged temperature versus height z in the OB and NOB cases, respectively. The height of the cell is L . The temperature at the top plate $z = L$ is T_t and the one at the bottom plate $z = 0$ is T_b . The mean temperature is $T_m = (T_t + T_b)/2$. The thickness of the top thermal BL is λ_t , that of the bottom thermal BL is λ_b . The respective temperature drops are Δ_t and Δ_b . The time averaged temperature in the center is T_c . For water as the working fluid this center or bulk temperature T_c is larger than the mean temperature T_m . While $\lambda_{t,b}$ in the OB case are equal, under NOB conditions in the case of water the bottom BL is thinner as the top one, $\lambda_b < \lambda_t$. The z -dependence of Λ implies a (numerically small) curvature of the temperature profiles in the BLs. For $T_c > T_m$ the top BL width becomes larger and the bottom BL width smaller if OB is no longer valid. As will be discussed later, the sum of both widths at least for water seems to be the same as the corresponding sum under OB conditions. The relations between the slope-based BL thicknesses λ^{sl} and the profile based thicknesses $\lambda^{99\%}$ (“99% rule”) will be shown to be $\lambda_{t,b}^{sl} < \lambda_{t,b}^{99\%}$, as is apparent from the graph, cf. also subsection 6.2, in particular Figure 15.

density ρ and the isobaric specific heat capacity c_p per mass to a good approximation are temperature and therefore height independent. For the case of water between 20°C and 60°C, on which we will focus, this is given with a precision of 1.6% and 0.07%, respectively, see table 1. Thus in the following we always consider ρ and c_p as being

temperature $^{\circ}C$	$10^{-3}\rho$ $kg\ m^{-3}$	$10^{-3}c_p$ $J\ kg^{-1}K^{-1}$	$10^4\beta$ K^{-1}	Λ $W\ m^{-1}K^{-1}$	$10^6\kappa$ $m^2\ s^{-1}$	$10^6\nu$ $m^2\ s^{-1}$	Pr
$T_t = 20.000$	0.99809	4.175	2.05	0.5975	0.1448	1.004	6.94
$T_{\bar{t}} = 30.911$	0.99532	4.169	3.14	0.6162	0.1494	0.794	5.31
$T_m = 40.000$	0.99220	4.169	3.88	0.6297	0.1528	0.669	4.38
$T_c = 41.822$	0.99150	4.169	4.02	0.6322	0.1534	0.648	4.23
$T_{\bar{b}} = 50.911$	0.98761	4.173	4.64	0.6434	0.1563	0.557	3.57
$T_b = 60.000$	0.98316	4.178	5.21	0.6529	0.1590	0.485	3.05

TABLE 1. Fluid parameters for the medium cell of height $L = 24.76\ cm$ in the local gravity field (Santa Barbara) $g = 979,1\ cm\ s^{-1}$, with the top temperature $T_t = 20.00^{\circ}C$ and the bottom temperature $T_b = 60.00^{\circ}C$. The corresponding Rayleigh number is $Ra = 2.26 \cdot 10^{10}$ and the Prandtl number is $Pr = 4.38$, both based on the fluid parameters at the mean temperature $T_m = 40.00^{\circ}C$. This corresponds closely to the last data point for the medium cell in figure 9. The value $\chi = 0.833$ is obtained from the measured center temperature $T_c = 41.822^{\circ}C$. The mean temperatures $T_{\bar{t}}$ and $T_{\bar{b}}$ in the thermal top and bottom BLs are $T_{\bar{t}} = T_t + \Delta_t/2$ and $T_{\bar{b}} = T_b - \Delta_b/2$; the temperature drops follow from $\Delta_t = T_c - T_t$ and $\Delta_b = T_b - T_c$.

constant. All obtained results are considered as applicable to liquids, which share these properties $\rho = \text{constant}$ and $c_p = \text{constant}$.

Eq. (2.9) then means that the expression in rectangular brackets is z -independent and therefore defines the conserved thermal current

$$\langle u_z \theta \rangle_A - \kappa(z) \partial_z \langle \theta \rangle_A \equiv J. \quad (2.10)$$

Here $\kappa(z) = \Lambda(z)/\rho c_p$ is the thermal diffusivity. J is z -independent and interpreted as the thermal flux, connected with the heat flux Q by $J = Q/\rho c_p$. Making the thermal flux J or the heat flux Q dimensionless, we obtain the Nusselt number

$$Nu_m = Nu \equiv \frac{Q}{\Lambda_m \Delta/L} = \frac{J}{\kappa_m \Delta/L} = \frac{L}{\kappa_m \Delta} [\langle u_z \theta \rangle_A - \kappa(z) \partial_z \langle \theta \rangle_A]. \quad (2.11)$$

Again, Nu without label m refers to the flux as being nondimensionalized with the material parameter κ_m taken at the mean temperature T_m of the control temperatures at the plates.

2.4. Thermal boundary-layer thicknesses

As under OB conditions the boundary layer thickness in the NOB case can be defined in two ways. A theoretically convenient definition is via the slope of the temperature profile at the plate. As the thickness λ^{sl} of the boundary layer we take that distance from the plate, where the tangent to the temperature profile at $z = 0$ (or correspondingly at $z = L$) reaches the center temperature T_c .

From eq. (2.11) we have $Q = -\Lambda(T(z=0)) \partial_z \langle \theta \rangle_A(0)$. For given heat current Q the slopes at the top and bottom are different, because the Λ 's are different due to their temperature dependence. For $z > 0$ but in the immediate vicinity of the plates, where the convective contribution in (2.11) is still negligible, the slope $\partial_z \langle \theta \rangle_A$ already varies with z since $\Lambda(T(z))$ varies. Thus there is a curvature in the NOB profile which is absent in the OB case where Λ is height (z) independent.

Going e.g. from the bottom plate $z = 0$ into the interior of the RB cell, $\Lambda(z)$ decreases according to the material properties of water, given in Table 1. Therefore the slope $\partial_z \langle \theta \rangle_A$

increases and $\partial z / \partial \langle \theta \rangle$ as its inverse decreases. The profile thus first bends downwards (more parallel to the plate surface) before near the bulk range it more or less sharply bends upwards to merge into the constant center temperature T_c . This characteristic additional curvature of the profile, which *increases* the angle under which the temperature profile hits the bottom plate surface, is a signature of NOB conditions in the thermal boundary layer. In comparison to the OB case the slope $\partial \langle \theta \rangle / \partial (-z) = Q/\Lambda$ is smaller in the NOB case, since Λ is larger at the bottom temperature T_b . In contrast, at the cooler top plate the slope becomes larger under NOB conditions because of the smaller Λ , and thus the angle to the plate surface here decreases. This breaks the symmetry of the temperature profile in the z -direction about the horizontal midplane of the cell. In figure 1 we have sketched the BL temperature profiles for the OB and NOB cases. (Near onset of convection this broken midplane symmetry is one of the important factors for pattern formation under NOB conditions, which is different from the OB case, cf. Busse (1967).) These findings about the temperature profile changes are still open for experimental verification.

Now, by definition, the flux conservation equation (2.11) for the heat flux Q or thermal flux J implies a relation between the ratios of these BL thicknesses $\lambda_b^{sl}, \lambda_t^{sl}$ and the corresponding temperature drops Δ_b, Δ_t . Namely, applying equation (2.10) or (2.11) at the two plates $z = 0$ and $z = L$ gives

$$\kappa_t \frac{\Delta_t}{\lambda_t^{sl}} = \kappa_b \frac{\Delta_b}{\lambda_b^{sl}} = J = Nu \frac{\kappa_m \Delta}{L}. \quad (2.12)$$

In analogy to the ratio χ of the temperature drops (cf. eq. (2.4)) we also introduce the ratio of the slope BL thicknesses

$$\chi_{\lambda^{sl}} = \frac{\lambda_b^{sl}}{\lambda_t^{sl}} = \frac{\kappa_b}{\kappa_t} \frac{\Delta_b}{\Delta_t} = \frac{\kappa_b}{\kappa_t} \chi = \chi_\kappa \chi, \quad (2.13)$$

which is another measure characterizing NOB effects. Here χ_κ is the ratio

$$\chi_\kappa = \kappa_b / \kappa_t, \quad (2.14)$$

and χ_ν, χ_β , etc. are similarly defined.

For the thicknesses of the BLs themselves one has from eqs. (2.12) and (2.6),(2.7)

$$\frac{\lambda_b^{sl}}{L} = \frac{\Delta_b}{\Delta} \frac{\kappa_b}{\kappa_m} \frac{1}{Nu} = \frac{\chi}{1 + \chi} \frac{\kappa_b}{\kappa_m} \frac{1}{Nu}, \quad (2.15)$$

$$\frac{\lambda_t^{sl}}{L} = \frac{\Delta_t}{\Delta} \frac{\kappa_t}{\kappa_m} \frac{1}{Nu} = \frac{1}{1 + \chi} \frac{\kappa_t}{\kappa_m} \frac{1}{Nu}. \quad (2.16)$$

By adding these two equations one easily obtains for the Nusselt number

$$Nu = \frac{L}{\lambda_t^{sl} + \lambda_b^{sl}} \frac{\kappa_t \Delta_t + \kappa_b \Delta_b}{\kappa_m \Delta}. \quad (2.17)$$

Another way to define the thermal BL thickness takes the full temperature profile of the BL into account. It defines the thermal BL thickness $\lambda^{99\%}$ as that distance from the plate, at which the temperature is near the center temperature, e.g. if at the bottom $T = T_b - 0.99\Delta_b$ is achieved. This definition is in analogy to the definition of the thickness δ of the kinetic BL, defined by the distance where, say, 99% of the bulk velocity is achieved.

In the OB case this profile-based thickness δ of the kinetic BL follows from the classical

Prandtl-Blasius theory (Prandtl (1905); Blasius (1908)),

$$\delta = aL/Re^{1/2}. \quad (2.18)$$

In Grossmann & Lohse (2002) we have determined the prefactor a for the case of flow in RB cells from the experimental results of Qiu & Tong (2001*b*), leading to $a = 0.483$. (This value differs, of course, from the Blasius factor, valid for flow along infinite plates.) Under OB conditions the profile-based thermal boundary-layer thickness $\lambda^{99\%}$ can be calculated according to the Prandtl-Blasius BL theory (cf. Meksyn (1961); Schlichting & Gersten (2000)). It is (cf. also Grossmann & Lohse (2004))

$$\frac{\lambda^{99\%}}{L} = \frac{a' C(Pr)}{Re^{1/2} Pr^{1/3}} \quad (2.19)$$

with a function $C(Pr)$ given by Meksyn (1961). For large Pr numbers one has $C(Pr) \rightarrow 1$, whereas for small Pr one finds $C(Pr) \propto Pr^{-1/6}$. The prefactor a' in principle can be different from the prefactor a of eq. (2.18).

While $\lambda^{99\%}/\delta \propto C(Pr)/Pr^{1/3}$ depends on Pr only, the corresponding ratio $\lambda^{sl}/\delta \propto \sqrt{Re}/Nu$ depends on both Pr and Ra in general. From the above profile discussion we expect $\lambda^{99\%} > \lambda^{sl}$. In section 6 this expectation will turn out to be correct.

Apparently the flow in the BLs of large Ra number RB flow will be time dependent. There are lots of BL separations and plume formations. Thus also the terms $\partial_t \theta$ in the heat conservation equation (2.8) and $\partial_t u_i$ in the Navier-Stokes equation for momentum conservation

$$\partial_t u_i + u_j \partial_j u_i = -\partial_i \frac{p}{\rho} + \partial_j (\nu \partial_j u_i) \quad (2.20)$$

will contribute. The flow is no longer laminar time independent. But apparently the overwhelming amount of RB data is consistent with the assumption that still the characteristic Prandtl scaling of the wall normal quantities holds, $z \propto L/\sqrt{Re}$ and $u_z \propto U/\sqrt{Re}$. The boundary layer flow is not yet fluctuation dominated as it is in fully developed turbulence, where the profile is expected to be adequately described by a logarithmic profile.

The formulas (2.4), (2.5), (2.6), and (2.7) represent our description of the basic features of the temperature profile. Equations (2.8), (2.9), (2.10), and (2.11) are consequences of the local conservation of heat. Equations (2.12) and (2.15),(2.16) contain additional physics, namely the definition of the BL thicknesses λ_b^{sl} and λ_t^{sl} . They reflect the fact that the heat transport into the liquid at the entrance $z = 0$ and out of the liquid at the exit $z = L$ is purely molecular and convection does not yet contribute. Note that the profile thicknesses $\lambda_{b,t}^{99\%}$ instead contain the influence of convection, represented by $\langle u_z \theta \rangle_A$.

3. Experimental results

3.1. Experimental setup

The experiments were done using three cylindrical cells filled with water. In each cell we made measurements of the quantities characterizing NOB effects at constant mean temperature T_m and thus constant mean Pr . In each case the aspect ratio $\Gamma \equiv D/L$ was close to one. The cells had heights $L = 50.62, 24.76, \text{ and } 9.52 \text{ cm}$, and diameters $D = 49.70, 24.81, \text{ and } 9.21 \text{ cm}$, corresponding to $\Gamma = 0.982, 1.002, \text{ and } 0.967$. We will refer to them as the large, medium, and small cell respectively. For most of the measurements the mean temperature was $T_m = 40.00^\circ\text{C}$ where $Pr = 4.38$; for some it was 29°C where $Pr = 5.55$. We varied Ra by varying Δ at fixed T_m thus keeping all other parameters in

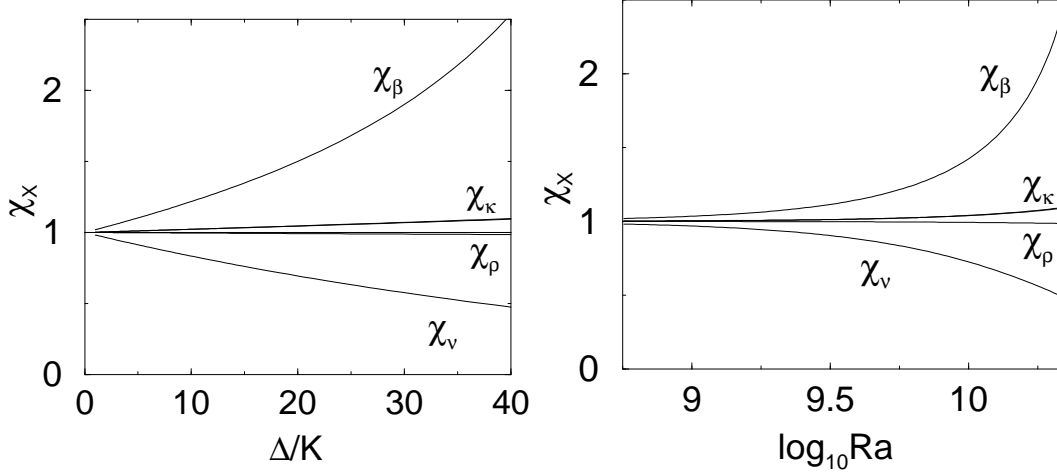


FIGURE 2. The ratios χ_X of the material parameters for $T_m = 40^\circ\text{C}$ at the bottom and top walls as functions of Δ (left), or as functions of $Ra = \Delta/\Delta_{m,medium}$ (right) for the medium cell. It is $\Delta_{m,medium} = 1.772 \times 10^{-9} K$. The symbol X stands for β , κ , ρ , or ν . χ_Λ is indistinguishable from χ_κ , and both χ_ρ and $\chi_{c\rho}$ are basically equal to 1. Deviations from $\chi_X = 1$ signal NOB effects. The ratio can be larger than 2 (smaller than 1/2) for χ_β (χ_ν). Evident consequences are significant differences of the buoyancy force, of the viscous drag, and thus of the BL thickness near the bottom as compared with the top region. A nonlinear dependence of the various χ_X 's on Δ seems apparent.

the definition (2.1) of Ra fixed. Therefore Ra here means $Ra = \Delta/\Delta_{m,i}$, with $\Delta_{m,i} = \nu_m \kappa_m / \beta_m g L_i^3$ where the label i means “large”, “medium”, or “small” cell. Time-averaged values of the top-plate temperature T_t , the bottom-plate temperature T_b , and the heat current Q were obtained at each Ra . For the medium and large cell we also determined T_c by measuring the side-wall temperature at half-height using eight thermometers at uniformly distributed azimuthal locations. All measurements were averaged over time periods ranging from slightly less than a day to several days. For each Ra value the side-wall temperatures were averaged over the eight locations. Since there is virtually no heat flow laterally through the wall, we expect the side-wall temperature to be equal to the temperature of the fluid adjacent to it. Because of the large-scale circulation (LSC), the fluid temperature varies along a diameter of the horizontal mid-plane, being higher where the fluid rises and lower where it falls. Qiu & Tong (2001a) made temperature measurements for a slightly tilted cell with $\Gamma = 1.07$ and $L = 20.3\text{ cm}$ in which the LSC had a preferred angular orientation determined by the tilt direction. Along a diameter oriented to coincide with the tilt direction they showed that the temperature variation is linear. For a Rayleigh number of 3.3×10^9 ($\Delta = 16\text{ K}$) they found it to be $\delta T \simeq 0.12\text{ K}$ across the radius, giving $\delta T/\Delta \simeq 0.0075$. Because of the linear variation of T along the diameter, we expect the average temperature given at two opposite locations to be equal to the center temperature T_c to better than 0.1% of Δ . Since we averaged the readings of eight thermometers uniformly distributed around the azimuth, we believe that our side-wall temperature-readings give an accurate determination of T_c . We note that such a determination can not be done accurately with a single thermometer, as was attempted by Chillà *et al.* (2004). For details regarding the experimental apparatus and procedures, see Brown *et al.* (2005).

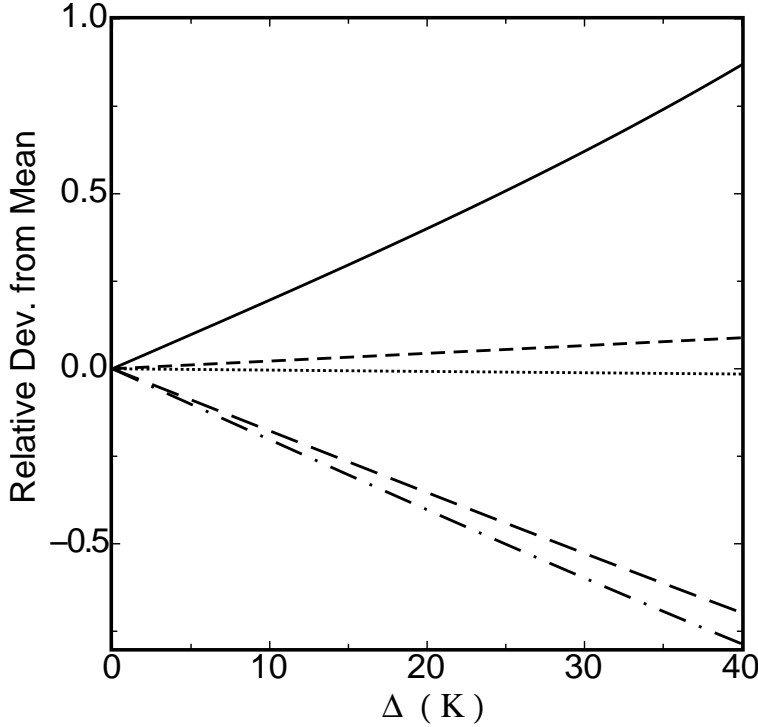


FIGURE 3. The relative deviation $2(X_b - X_t)/(X_b + X_t)$ of a property X from its mean value $(X_b + X_t)/2$ as a function of the temperature difference Δ for a mean temperature $T_m = 40^\circ\text{C}$. Solid line: expansion coefficient β . Short dashed line: heat conductivity λ and thermal diffusivity κ . Dotted line: density ρ . Long dashed line: kinematic viscosity ν . Dash-dotted line: Prandtl number Pr .

3.2. Temperature measurements

The ratios $\chi_\kappa, \chi_\nu, \chi_\beta, \dots$ (see e.g. equation (2.14)) characterize the strength of the NOB effects from the material properties. For the Δ range covered in the medium and small cell, these effects can be considerable, as seen from Fig. 2. In particular, this holds for the kinematic viscosity, which at the top wall is more than twice as large than at the bottom wall, and for the thermal expansion coefficient β , which at the top wall is less than 1/2 of its value at the bottom wall. The effect on χ_κ and χ_λ is up to 8%, whereas it is negligibly small for the density ρ and the specific heat capacity c_p . Figure 3 displays the *relative* deviations $2(X_b - X_t)/(X_b + X_t)$ of the various material properties. A similar analysis of the properties of the helium gas used for Nusselt-number measurements in cryogenic experiments was carried out by Niemela & Sreenivasan (2003) (see their Fig. 6). In the helium case the major contribution to NOB effects comes from c_p and β ; unlike for water, the viscosity plays only a minor role.

In Fig. 4 we show the temperature differences $\Delta_b = T_b - T_c$ (circles) and $\Delta_t = T_c - T_t$ (squares) for $Pr = 4.38$. The open (solid) symbols are for the medium (large) cell. The increasing difference between Δ_b and Δ_t with increasing Δ reflects the growing deviation from the Oberbeck-Boussinesq approximation; for OB conditions one would have $\Delta_b = \Delta_t = \Delta/2$. In Fig. 5 we show half this difference, equal to $T_c - T_m$, as a function of Δ for $Pr = 4.38$ as well as for $Pr = 5.55$. Figure 6 gives the experimental results for $\chi = (T_b - T_c)/(T_c - T_t) = \Delta_b/\Delta_t$ for the large (solid symbols) and medium (open symbols) cell for $Pr = 4.38$ (circles) and for $Pr = 5.55$ (squares). In Fig. 7 we replot

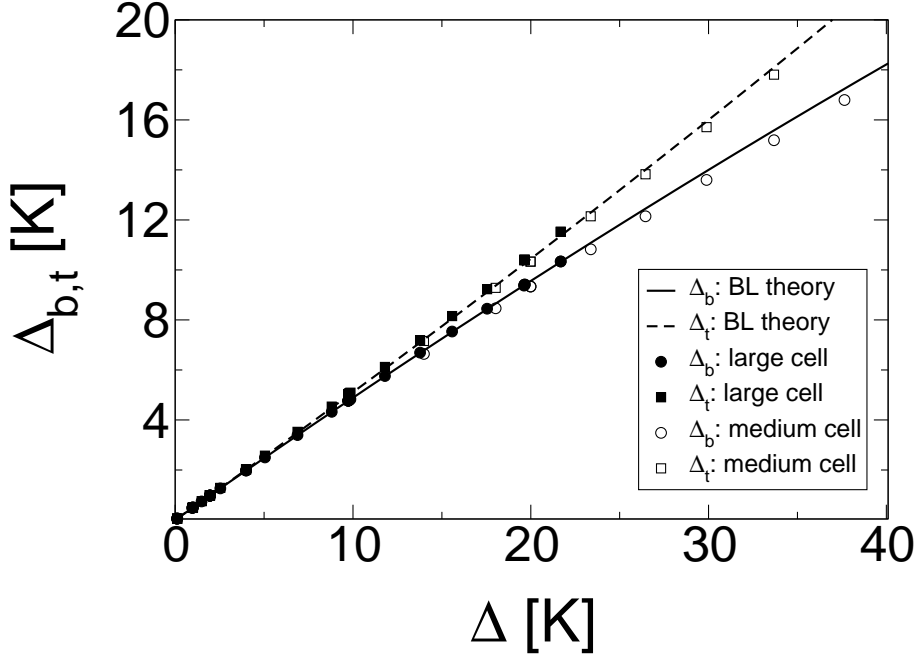


FIGURE 4. The measured temperature differences $\Delta_b = T_b - T_c$ (circles) across the bottom and $\Delta_t = T_c - T_t$ (squares) across the top BL for $T_m = 40.00^\circ\text{C}$ ($Pr = 4.38$) as a function of the total applied temperature difference Δ . Solid symbols: large cell. Open symbols: medium cell. The solid and the dashed lines originate from our theory presented in section 6.

χ as a function of Ra for the medium cell and $Pr = 4.38$. In Figs. 5 and 6 equations for polynomial fits to the data are given in the caption. In section 5 we will compare our experimental results for χ with the prediction of Wu & Libchaber (1991), based on the assumption of equal temperature scales at the bottom and the top boundary layers. As can be seen already from Fig. 6, this prediction does not agree very well with our data.

3.3. NOB effects on Nu and Re

We now come to the NOB effects on the Nusselt number Nu and the Reynolds number Re . For each L the data covered about 1.5 decades of Ra . However, since $Ra \propto L^3 \Delta$, the Ra -range of each cell was shifted relative to the next larger or smaller one by about a decade. The measurements at the largest Ra of a smaller cell, which might be expected to show departures of Nu and Re from the OB approximation, overlapped with results at the smallest Ra of a larger cell which in turn would be expected to conform well to the OB approximation. Thus a comparison between any two cells in the overlapping range of Ra can be expected to reveal NOB effects.

The Reynolds number Re of the large-scale circulation, deduced from plume transit times, is measured via temperature auto- and cross-correlations, as detailed by Brown *et al.* (2006). The velocity U , on which Re is based via eq. (2.3), is measured as a distance, proportional to the cell height L , divided by the turnover time of the plumes. In the OB case Re is found to scale like $Ra^{0.46}$ up to $Ra \simeq 2 \cdot 10^9$, and beyond that critical Rayleigh number like $Ra^{1/2}$. Here we focus only on possible NOB effects on Re . For that we show in figure 8 the experimental results for $Re/Ra^{1/2}$ vs Ra . The solid squares (medium cell) near $Ra = 2.1 \cdot 10^{10}$ are for $\Delta = 38\text{K}$ and should show NOB effects, whereas those for the large cell (open symbols) at the same Ra are for $\Delta \approx 4.4\text{K}$, clearly in the OB range.

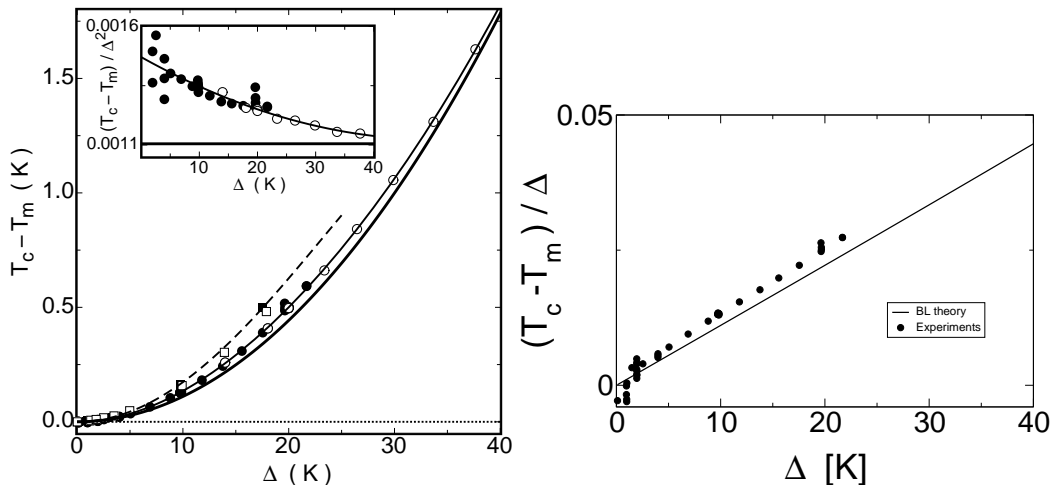


FIGURE 5. (a) The difference between the measured temperature T_c at half-height and the mean (control) temperature $T_m = (T_b + T_t)/2$. Solid symbols: large cell. Open symbols: medium cell. Circles: $T_m = 40^\circ\text{C}$ and $Pr = 4.38$. Squares: $T_m = 29^\circ\text{C}$ and $Pr = 5.55$. The solid (dashed) line corresponds to the polynomial fit $T_c - T_m = c_2\Delta^2 + c_3\Delta^3 + c_4\Delta^4$ to the large (medium) cell data with $c_2 = 1.47 \times 10^{-3} \text{K}^{-1}$ ($c_2 = 1.81 \times 10^{-3} \text{K}^{-1}$), $c_3 = -1.37 \times 10^{-5} \text{K}^{-2}$ ($c_3 = -1.81 \times 10^{-5} \text{K}^{-2}$), $c_4 = 1.35 \times 10^{-7} \text{K}^{-3}$ ($c_4 = 0$). The fat line results from our theory of section 6, applied to the large cell. Its polynomial representation yielded $c_2 = 1.105 \times 10^{-3} \text{K}^{-1}$, $c_3 = 1.09 \times 10^{-8} \text{K}^{-2}$, and $c_4 = 5.79 \times 10^{-9} \text{K}^{-3}$. Although c_3 and c_4 are much smaller than the experimental values, the overall curve is in quite good agreement with the data. The center temperature T_c deviates from T_m by 1.822K for $\Delta = 40\text{K}$, i.e., by less than 5%. Thus the comparison between theory and experiment is easier if one plots the quantity $(T_c - T_m)/\Delta^2$, in K^{-1} , vs. Δ , as done in the inset (again the solid and the fat line are the fit to the data and the theory respectively). Figure (b) displays the dimensionless quantity $(T_c - T_m)/\Delta$ vs. Δ for the large cell only.

For each of the two cells, the extent of departures of T_c from the OB approximation T_m is illustrated in the lower figure by the temperature ratio $\chi = \frac{\Delta_b}{\Delta_t} = \frac{\Delta/2 - (T_c - T_m)}{\Delta/2 + (T_c - T_m)}$. As the two sets of data for Re agree within the experimental precision (about 2%), it can be concluded that NOB effects on Re for $\chi \simeq 0.84$ are at most a percent or two.

The Nu data for the large and medium cells were corrected for the effect of the finite conductivity of the copper top and bottom plates [Chaumat *et al.* (2002); Verzicco (2004); Brown *et al.* (2005); Nikolaenko *et al.* (2005)] on the heat transport in the fluid (no correction was needed for the small cell). The influence of the finite wall conductivity [Ahlers (2000); Roche *et al.* (2001); Verzicco (2002); Niemela & Sreenivasan (2003)] was negligible, except for the small cell where a correction of order one percent was applied. These experiments are described in detail by Brown *et al.* (2005). Data for $Nu(Ra)$ under strictly Boussinesq (OB) conditions were reported by Funfschilling *et al.* (2005). Here we concentrate on the results relevant to deviations from the OB approximation.

One may wonder whether the weak deviation of the aspect ratio from 1 ($\Gamma = 0.982, 1.002, 0.967$ for the large, medium, and small cell, respectively) may affect our results on the Nusselt number, as Shraiman & Siggia (1990) had suggested a relatively strong aspect ratio dependence $Nu \sim \Gamma^{-3/7}$. However, note that the actual dependence is much weaker as demonstrated experimentally by the work of Funfschilling *et al.* (2005). There it is shown for instance that the $\Gamma = 6$ results for Nu are only about 4% below the $\Gamma = 1$ results. This extremely small Γ dependence was confirmed more recently also by Sun *et al.* (2005). It can not influence the present data over the range $0.967 \leq \Gamma \leq 1.002$ by a measurable

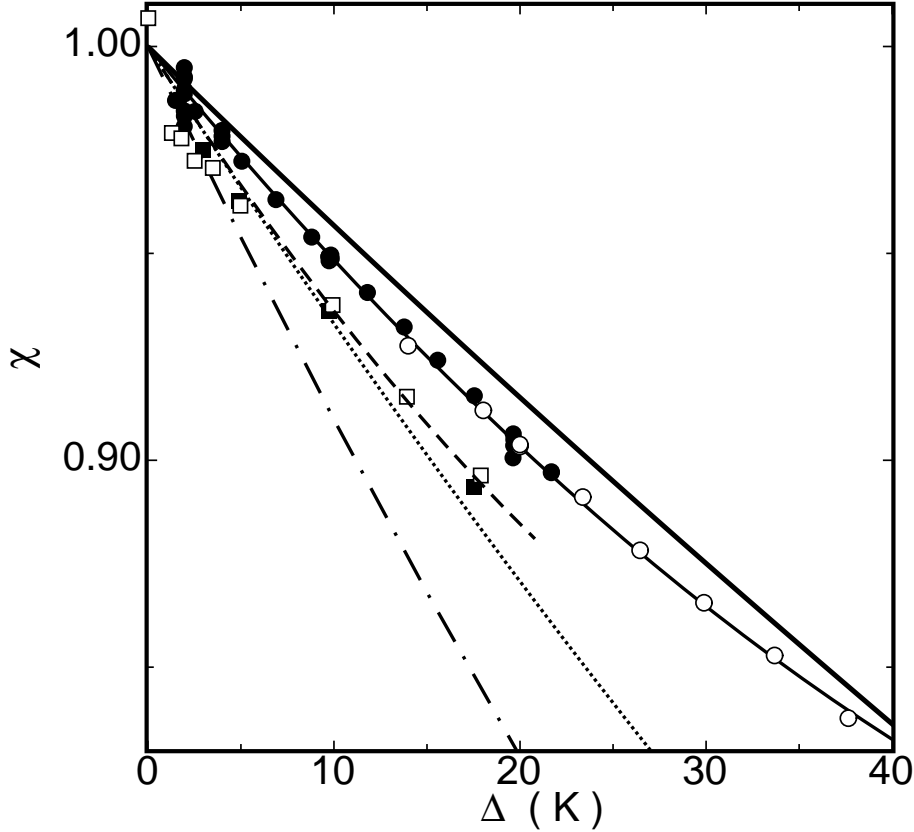


FIGURE 6. Experimental results for the ratio $\chi = (T_b - T_c)/(T_c - T_t) = \Delta_b/\Delta_t$ for the large cell (solid symbols) and medium cell (open symbols). Circles: $T_m = 40.00^\circ\text{C}$ and $Pr = 4.38$. Squares: $T_m = 29.00^\circ\text{C}$ and $Pr = 5.55$. The solid (dashed) line is a polynomial fit to the data that yielded $\chi = 1 + a_{\chi,1}\Delta + a_{\chi,2}\Delta^2$ with $a_{\chi,1} = -5.48 \times 10^{-3}\text{K}^{-1}$ and $a_{\chi,2} = 3.25 \times 10^{-5}\text{K}^{-2}$ ($a_{\chi,1} = -7 \times 10^{-3}\text{K}^{-1}$ and $a_{\chi,2} = 6 \times 10^{-5}\text{K}^{-2}$). The dotted and dash-dotted lines are the results computed for $T_m = 40.00$ and 29.00°C respectively from Eq. (5.4) as suggested by Wu & Libchaber (1991). They can be represented by $\chi_{WL} = 1 - 0.00694\Delta + 2.38 \times 10^{-5}\Delta^2$ and $\chi_{WL} = 1 - 0.00945\Delta + 4.35 \times 10^{-5}\Delta^2$, respectively. In our data the linear terms seem dominant, but the nonlinear deviations are clearly visible. For $\Delta = 40\text{K}$ the contributions are $1 - 0.219 + 0.052$. The fat line results from our theory of section 6, applied to the large cell. It is in reasonable agreement with the data.

amount. However, we have corrected for tiny systematic errors in the data as discussed already by Funfschilling *et al.* (2005) (due primarily to errors in the geometry) which can be different for different cells (by a fraction of a percent) by overlapping the Nusselt numbers (through tiny shifts) of the small and the medium cell and then of the medium and the large cell in their respective BO regimes.

In Fig. 9a we show the results for Nu in the reduced form of $Nu/Ra^{1/3}$ as a function of Ra (on a logarithmic scale). For the small and medium cell, one sees that Nu in the NOB region is slightly smaller, but only by a percent or so, than the data in the strictly Boussinesq range.

In order to show the NOB effect more clearly, we fitted the strictly Oberbeck-Boussinesq

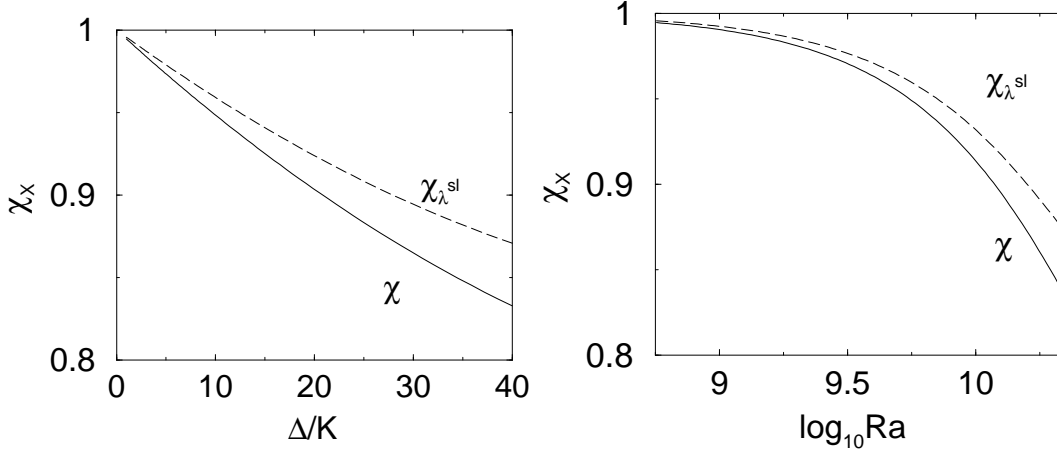


FIGURE 7. The ratios $\chi = \chi_\Delta$ (solid) and $\chi_{\lambda^{sl}}$ (dashed) at $T_m = 40^\circ\text{C}$ and $Pr = 4.38$ as functions of Δ (left), and as functions of $Ra = \Delta/\Delta_{m,medium}$ for the medium cell (right), with $\Delta_{m,medium} = \nu_m \kappa_m / (\beta_m g L_{medium}^3) = 1.772 \times 10^{-9} \text{K}$. Deviations from $\chi_X = 1$ signal NOB effects.

data (Funfschilling *et al.* (2005)) to the empirical function

$$Nu/Ra^{0.3} = \sum_{i=0}^4 b_i [\log_{10}(Ra)]^i \quad (3.1)$$

and obtained the coefficients $b_0 = -1.7934$, $b_1 = 0.85734$, $b_2 = -0.13992$, $b_3 = 0.009902$, $b_4 = 0.0002490$. The function fits the data within their scatter, but should not be relied upon for Ra values outside the range $10^8 < Ra < 10^{11}$ used in the fit. Relative deviations from the function are shown in Fig. 9b. There the deviations from the OB approximation become more clear. In figure 10 the same data for Nu_{NOB}/Nu_{OB} are given as a function of Δ .

Comparison with Figs. 6 and 7 shows that NOB effects on Nu are negligible in the range where $\chi \gtrsim 0.94$ but detectable in the experiment for smaller values of χ , i.e., for larger NOB deviations from $\chi = 1$. But even when χ reaches its smallest experimental value near 0.83, the data fall less than only 1.5 percent below the Boussinesq results. Even though the NOB effects on Nu are quite small, it is interesting to note that they *diminish* the heat transport.

Measurements of χ and of Nu under NOB conditions were made before by Wu & Libchaber (1991) using ^4He gas at low temperatures near its critical point. For small Ra , where their cells conformed to the Oberbeck-Boussinesq approximation, they found $\chi \simeq 1.1$. It is not known why their results in this OB limit differed systematically from unity. At large Ra , however, their results for χ became as large as 2.5, indicating strong NOB effects. They did not have two cells of different sizes, and thus of different departures from the OB approximation at the same Ra , for comparison. However, when their data were plotted on a log-log scale, the results at large Ra fell significantly below a straight line drawn through the results at smaller Ra . Assuming that a power-law should have fit the OB data, one then can conclude that also in this case Nu decreased due to NOB effects.

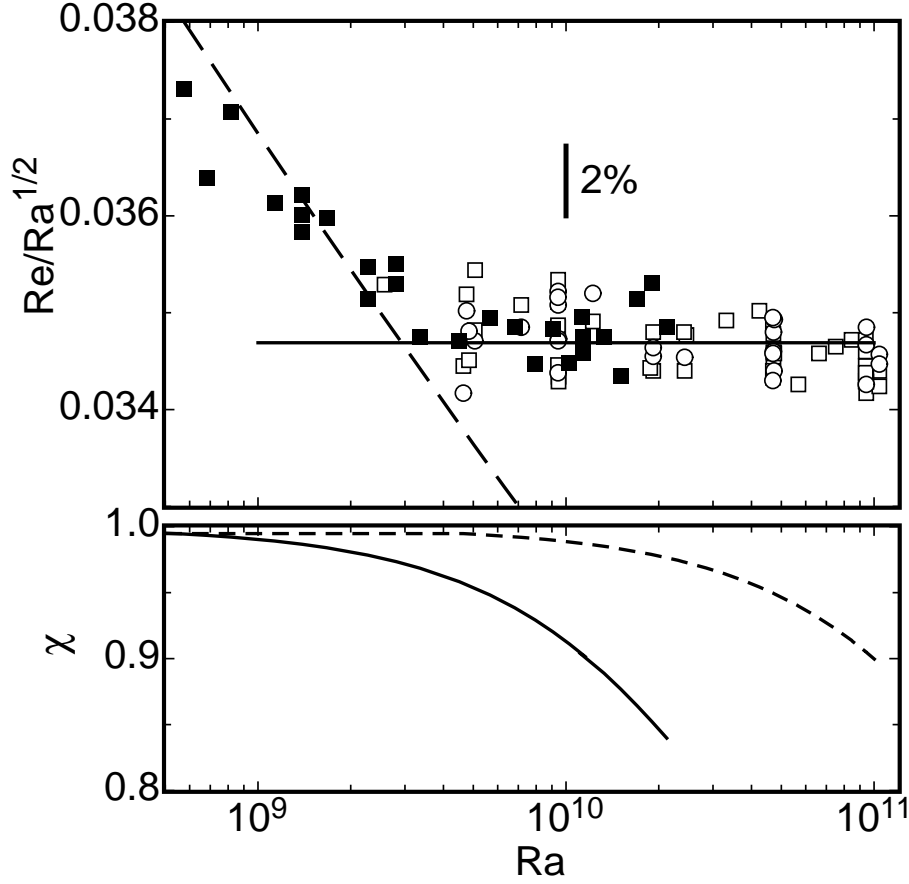


FIGURE 8. Upper figure: $Re/Ra^{1/2}$ vs Ra as measured for the medium cell (solid symbols) and the large cell (open symbols). (The dashed and solid lines indicate the change of the Ra -dependence of Re which is not discussed here.) Lower figure: $\chi = \Delta_b/\Delta_t$ as a function of Ra for the medium (solid line) and large (dashed line) cell. The square-symbols originate from the cross-correlations, the circle-symbols from auto-correlations of temperatures. The solid squares (medium cell) at the highest Ra ($Ra = 2.1 \cdot 10^{10}$) are for $\Delta = 38K$, have $\chi \simeq 0.84$, and should show NOB effects, whereas those for the large cell at the same Ra (open symbols), which are for $\Delta \approx 4.4K$, have $\chi \simeq 0.98$, and are clearly in the OB range. As the two data sets agree within the experimental precision (2%), it can be concluded that NOB effects on Re are at most of that order of magnitude for χ near 0.84.

4. Towards understanding the NOB robustness of Nu

Can one understand the insensitivity of Nu to the NOB conditions, which so strongly contrasts with the sensitivity of the ratios χ_ν , χ_β for the material properties, or for the ratio $\chi = \Delta_b/\Delta_t$? The center temperature T_c deviates from the mean temperature T_m by about 5% at $\Delta = 40K$, i.e., also is rather insensitive. A step towards an understanding is to divide the Nusselt number Nu in the form eq. (2.17) by its OB value $Nu_{OB} = L/(2\lambda_{OB}^{sl})$. This gives

$$\frac{Nu_{NOB}}{Nu_{OB}} = \frac{2\lambda_{OB}^{sl}}{\lambda_t^{sl} + \lambda_b^{sl}} \frac{\kappa_t \Delta_t + \kappa_b \Delta_b}{\kappa_m \Delta}. \quad (4.1)$$

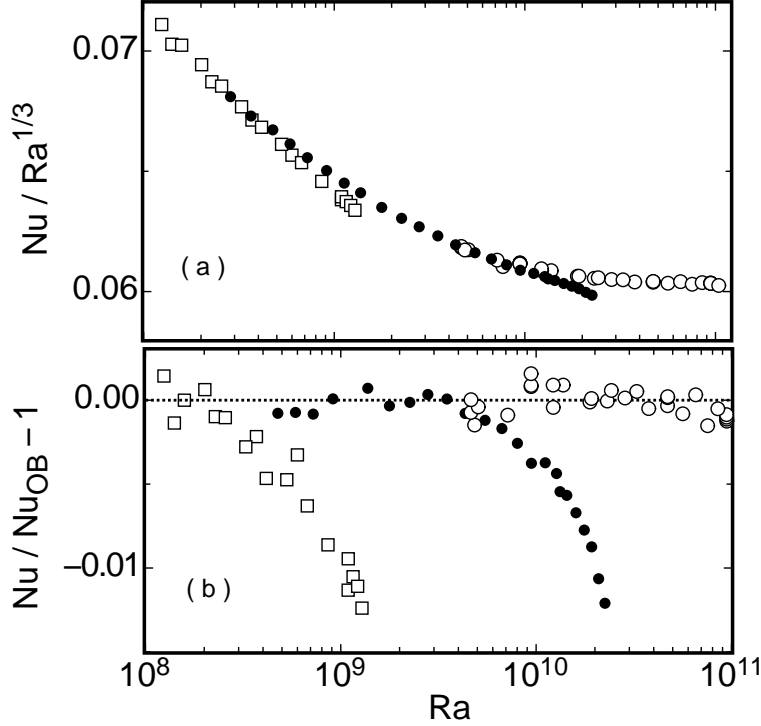


FIGURE 9. (a) The reduced Nusselt number $Nu/Ra^{1/3}$ on a linear scale as a function of the Rayleigh number Ra on a logarithmic scale for the small (open squares), medium (solid circles), and large (open circles) cell for $T_m = 40^\circ\text{C}$ ($Pr = 4.38$). For the small (medium) cell deviations from the Oberbeck-Boussinesq approximation are seen at the largest Ra and yield Nusselt numbers that are smaller than the more nearly Oberbeck-Boussinesq results obtained from the medium (large) cell. (b) The relative deviations of Nu from Eq. 3.1 as a function of Ra . This equation provides a good fit to the data taken under OB conditions in the Ra -range considered here. In Fig. 10 the same data for Nu_{NOB}/Nu_{OB} are given as a function of Δ .

(For clarity in this section we denote the measured Nusselt number Nu as Nu_{NOB} .) This ratio consists of two factors. In the first one

$$F_1 = \frac{2\lambda_{OB}^{sl}}{\lambda_t^{sl} + \lambda_b^{sl}}, \quad (4.2)$$

describing the contributions of the top and bottom thermal BL thicknesses, only the sum of the respective BL thicknesses in the OB and the NOB cases appears. Similarly, also in the second factor

$$F_2 = \frac{\kappa_t \Delta_t + \kappa_b \Delta_b}{\kappa_m \Delta} \quad (4.3)$$

the corresponding sums $\kappa_t \Delta_t + \kappa_b \Delta_b$ and $\kappa_m (\frac{\Delta}{2} + \frac{\Delta}{2})$ appear. In both factors F_1 and F_2 the NOB effects will increase one term and decrease the other term in the respective sums. If the material parameters depended on temperature only linearly, then there would be a (partial) cancellation of the NOB effects in the two terms, leading to only small NOB, order Δ^2 , corrections. This point will be made quantitative in subsection 6.4. Thus NOB

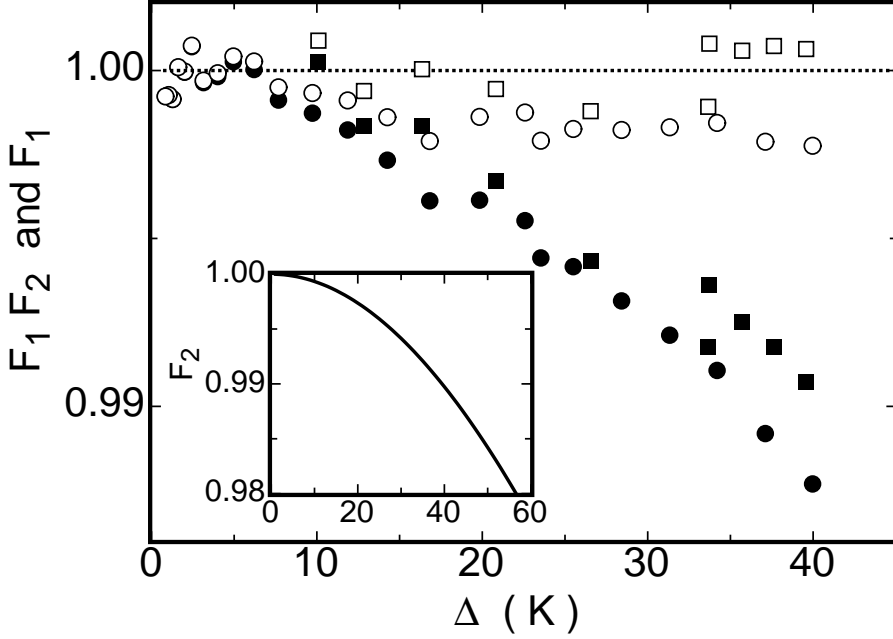


FIGURE 10. $F_1 \times F_2 = Nu_{NOB}/Nu_{OB}$ and F_1 (defined by equation (4.2) but calculated via eq. (4.4), second equality sign) as functions of Δ . Solid circles: $F_1 \times F_2$ for the medium cell. Open circles: F_1 for the medium cell. Solid squares: $F_1 \times F_2$ for the small cell. Open squares: F_1 for the small cell. While the product $F_1 \times F_2$ is the measured ratio of the heat currents Q in the NOB case and that in the OB case, the individual factors F_1 and F_2 contain the material properties, in particular F_2 depends on $\kappa(T)$ together with χ according to eq.(4.3). The inset shows the parameter $F_2 = (\kappa_t \Delta_t + \kappa_b \Delta_b)/(\kappa_m \Delta)$ as a function of Δ for $T_m = 40^\circ\text{C}$. The input is the material parameter $\kappa(T)$ and the measured ratio $\chi = \Delta_b/\Delta_t$. The equation $F_2 = 1 + d_2\Delta^2 + d_3\Delta^3$ with $d_2 = -6.81 \times 10^{-6} \text{K}^{-2}$ and $d_3 = 0.98 \times 10^{-8} \text{K}^{-3}$ yielded a good fit to the data.

corrections of Nu depend on the nonlinear, at least quadratic contributions to the NOB deviations of the material parameters, in contrast to those of χ or $(T_c - T_m)/\Delta$, χ_ν , and χ_β , which have already linear contributions. From figure 2, left, and figure 3 we conclude that at least for not too large Δ the Δ -dependence of the material properties indeed is basically linear, and we therefore start to understand the robustness of Nu towards NOB corrections: Linear NOB contributions cancel in Nu .

Let us focus on the Δ -dependence of the factors F_1 and F_2 in eq. (4.1) in more detail. From the thermal diffusivity $\kappa(T)$ and the experimental results for Δ_t and Δ_b we obtain $F_2(\Delta)$, see the inset of Fig. 10. As was the case for $T_c - T_m$, the factor F_2 can be well represented by the quadratic equation $F_2 - 1 = d_2\Delta^2$, without any linear term (plus of course higher powers of Δ). A least-squares fit to the data yielded $d_2 = -6.81 \times 10^{-6} \text{K}^{-2}$. We will theoretically understand this quadratic dependence in subsection 6.4.

With this F_2 and using the experimental results for Nu_{NOB}/Nu_{OB} from figure 10 we can calculate

$$F_1 = \frac{2\lambda_{OB}^{sl}}{(\lambda_t^{sl} + \lambda_b^{sl})} = \frac{Nu_{NOB}/Nu_{OB}}{F_2} = \frac{Q/Q_{OB}}{F_2}, \quad (4.4)$$

the ratio of the total thermal BL thicknesses. F_1 is displayed as open symbols in fig. 10. We see that within an experimental uncertainty of 0.2% the BL thickness ratio F_1 is independent of Δ , namely $F_1 \approx 1$. The experimental data thus suggest that $\lambda_t^{sl} + \lambda_b^{sl} \cong$

$2\lambda_{OB}^{sl}$ even under strong NOB conditions, where $\lambda_t^{sl}/\lambda_b^{sl}$ differs considerably from unity. Because of our finding for thermal convection in water, that the sum of the thermal slope BL thicknesses is conserved within experimental precision,

$$\lambda_t^{sl} + \lambda_b^{sl} \cong 2\lambda_{OB}^{sl} , \quad (4.5)$$

the NOB corrections on Nu are only governed by F_2 , and thus are quadratic in Δ to an extremely good approximation. The finding $F_2 < 1$ would then moreover explain the observed *reduction* of Nu_{NOB} as compared to Nu_{OB} .

Fig. 10 also shows $Nu_{NOB}/Nu_{OB} = F_1 \times F_2$ for the medium and small cell as solid circles and open squares, respectively. One sees that within 0.1% or so the data collapse onto a single curve.

We speculate on the meaning of these results and cautiously draw some very preliminary conclusions. Consider the hypothetical case that κ (and Λ) does not depend on T i.e., $\kappa_b = \kappa_t = \kappa_m$, while ν, β vary strongly. Then $F_2 = 1$ for any distribution of the temperature drops between top and bottom BL. Since for constant κ there is no additional curvature, the temperature profile will not lose its linear form in the BLs under NOB effects. Nevertheless, λ_b^{sl} can still be different from λ_t^{sl} , resulting in $T_c \neq T_m$. As long as the sum of the new BL thicknesses will be the same as it was before, i.e., under OB conditions, F_1 is equal to $F_1 = 1$. This immediately gives $Q_{NOB} = Q_{OB}$ or $Nu_{NOB} = Nu_{OB}$, i.e., the heat flow will not change despite $T_c \neq T_m$. The shift of the bulk temperature from T_m to T_c is the sole effect of the strong variations of ν and β , but Nu need not see this if κ is T -independent.

If, on the other hand, κ depends on T , there is additional profile curvature which will lead to a change of the heat flow Q . It seems as if F_2 takes care of that while still $F_1 \cong 1$. Then the non Oberbeck-Boussinesq heat current Q can be calculated solely from the material properties and the temperature drops Δ_b and Δ_t ,

$$\frac{Q_{NOB}}{Q_{OB}} = \frac{Nu_{NOB}}{Nu_{OB}} \cong \frac{\kappa_b \Delta_b + \kappa_t \Delta_t}{\kappa_m \Delta} . \quad (4.6)$$

This guarantees the robustness against NOB effects, because the linear term in the numerator is $\kappa_m \Delta$ and the cubic terms lead to corrections of order Δ^2 for the Q -ratio.

In the case of a curved profile the supposed condition $F_1 \cong 1$ could mean that the value of T_c has to adjust itself such that the sum of the BL thicknesses is invariant, i.e., that eq. (4.5) holds. The *volume* of the turbulent bulk then is invariant under deviations from OB conditions, only its time averaged temperature T_c takes notice of the NOB conditions and deviates from T_m . Certainly one has to check in further experiments (or with theoretical argument) if the constraint $\lambda_b^{sl} + \lambda_t^{sl} \cong 2\lambda_{OB}^{sl}$ also holds for other liquids than water in order to validate our finding. We do not know a physical reason why this should be the case in general; it may be incidental for water in the temperature range under investigation.

For a more thorough understanding of the robustness of Nu and also Re against NOB corrections more theoretical insight into the mechanism of the heat transport is required. Therefore we next consider RB convection models. We shall start with the first attempt to explain NOB effects, namely with the model of Wu and Libchaber (1991). It will turn out that their basic assumption is not consistent with the new data. We then, in Section 6, extend the Prandtl-Blasius boundary layer theory to T -dependent material parameters. It turns out that this can explain the experimental observations rather well.

5. Wu-Libchaber model for NOB effects

Wu & Libchaber (1991) and later Zhang *et al.* (1997) have studied the influence of deviations from OB conditions, both experimentally and by developing a model to cope with NOB effects on the Nusselt number. Their model extends the ideas of the Chicago scaling model for RB convection (Castaing *et al.* (1989)) by allowing for different temperature drops Δ_b and Δ_t at bottom and top. We shall briefly summarize the Wu-Libchaber (WL) results as far as relevant here, in our notation.

WL also use eq. (2.5), $\Delta_b + \Delta_t = \Delta$. Different top and bottom temperatures imply different thermal boundary-layer thicknesses, which they introduce by employing heat flux conservation

$$Q = \Lambda_{\bar{b}} \frac{\Delta_b}{\lambda_{\bar{b}}} = \Lambda_{\bar{t}} \frac{\Delta_t}{\lambda_{\bar{t}}} . \quad (5.1)$$

These BL thicknesses $\lambda_{\bar{b},\bar{t}}$ are defined in terms of the material properties, *taken at the mean temperatures* $T_{\bar{b}}$ and $T_{\bar{t}}$ in the respective BLs. These temperatures are $T_{\bar{b}} = T_c + \frac{\Delta_b}{2} = \frac{T_c + T_b}{2}$ and $T_{\bar{t}} = T_c - \frac{\Delta_t}{2} = \frac{T_c + T_t}{2}$.

Next, temperature scales θ_b and θ_t are introduced, characterizing the boundary layers in a different way than by the temperature drops Δ_b and Δ_t , namely

$$\theta_b = \frac{\nu_{\bar{b}} \kappa_{\bar{b}}}{g \beta_{\bar{b}} \lambda_{\bar{b}}^3} , \quad \theta_t = \frac{\nu_{\bar{t}} \kappa_{\bar{t}}}{g \beta_{\bar{t}} \lambda_{\bar{t}}^3} . \quad (5.2)$$

From their data (and later from the model of Zhang *et al.* (1997)) they concluded that these temperature scales should coincide†. Even more, in the framework of the model these scales are identified with the scale Δ_c of the temperature fluctuations in the bulk,

$$\theta_b = \theta_t = \Delta_c . \quad (5.3)$$

These equalities say that the BL thicknesses respond to the different temperature drops at bottom and top in such a way, that the thermal scales communicate through the thermal scale in the bulk. From eqs. (5.1), (5.2), and (5.3) one obtains

$$\chi = \frac{\Delta_b}{\Delta_t} = \frac{\Lambda_{\bar{t}} \lambda_{\bar{t}}}{\Lambda_{\bar{b}} \lambda_{\bar{b}}} = \frac{\kappa_{\bar{t}}}{\kappa_{\bar{b}}} \left(\frac{\beta_{\bar{t}} \nu_{\bar{b}} \kappa_{\bar{b}}}{\beta_{\bar{b}} \nu_{\bar{t}} \kappa_{\bar{t}}} \right)^{1/3} . \quad (5.4)$$

All material properties are to be taken at the middle temperature of the respective BL. In eq. (5.4) we have replaced the Λ -ratio by the κ -ratio because in water the additional factors ρ , c_p are practically temperature independent.

Since the temperatures $T_{\bar{b}}$ and $T_{\bar{t}}$ which are needed to evaluate the material parameters can be expressed in terms of χ , eq. (5.4) is an implicit equation for the temperature ratio χ . It can be solved iteratively (with fast convergence). The resulting Wu-Libchaber χ_{WL} for the case of water is plotted in Figure 6 for comparison with our measured data. Clearly, χ_{WL} is considerably smaller than found in experiment.

What is the origin of this shortcoming of the Wu-Libchaber model? To answer this we have to check the basic assumption eq. (5.3), on which (5.4) is based, i.e., on

$$\chi_\theta = 1 , \quad \text{where} \quad \chi_\theta \equiv \frac{\theta_b}{\theta_t} = \frac{\nu_{\bar{b}} \kappa_{\bar{b}} \beta_{\bar{t}}}{\nu_{\bar{t}} \kappa_{\bar{t}} \beta_{\bar{b}}} \cdot \chi_\lambda^{-3} = \frac{\nu_{\bar{b}} \kappa_{\bar{b}} \beta_{\bar{t}}}{\nu_{\bar{t}} \kappa_{\bar{t}} \beta_{\bar{b}}} \cdot \left(\frac{\kappa_{\bar{b}}}{\kappa_{\bar{t}}} \chi \right)^{-3} . \quad (5.5)$$

This, however, clearly is not the case, as seen from Fig. 11, which shows that χ_θ significantly deviates from $\chi_\theta = 1$. The idea of equal temperature scales θ_b and θ_t in the

† In the earlier work Wu & Libchaber (1991) in fact only assumed that θ_b and θ_t *scale* the same, and experimentally they found a ratio $\theta_b/\theta_t \neq 1$, independent of Ra , i.e., Δ . This, however, cannot be, as this ratio must become equal to 1 in the OB limit.

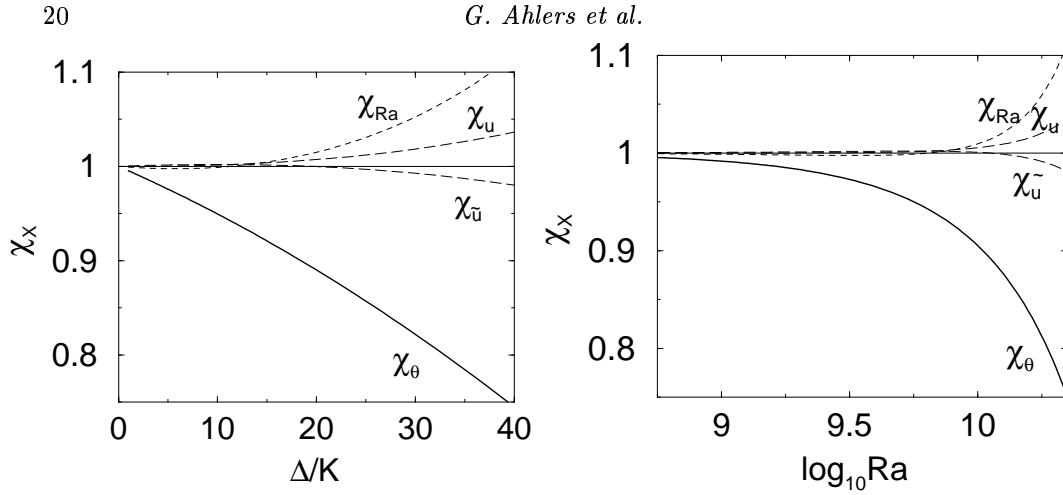


FIGURE 11. The ratios χ_θ (solid), χ_{Ra} (short-dashed), χ_u , $\chi_{\tilde{u}}$ (dashed), for water with $T_m = 40^\circ\text{C}$ and $Pr = 4.38$ as functions of Δ (left), and as functions of $Ra = \Delta/\Delta_{m,medium}$ for the medium cell (right). Deviations from $\chi_x = 1$ signal NOB effects. One sees that $\chi_\theta \neq 1$, in conflict with the assumption of Wu & Libchaber (1991) underlying their model of NOB effects.

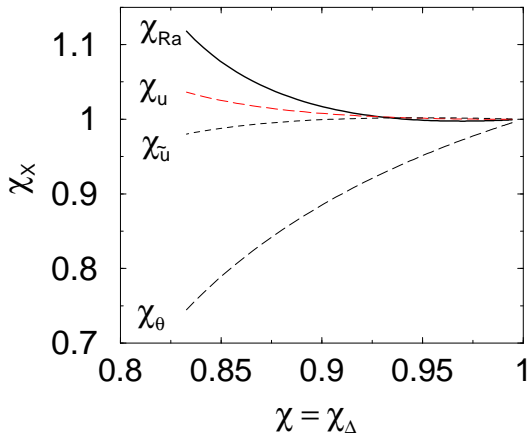


FIGURE 12. The same ratios χ_θ , χ_{Ra} , χ_u and $\chi_{\tilde{u}}$, as functions of the temperature drop ratio $\chi = \Delta_b/\Delta_t = \chi_\Delta$ for water and $T_m = 40^\circ\text{C}$.

bottom and top BLs is thus not consistent with experiment. For easier comparison with the corresponding Wu-Libchaber plot we show in Fig. 12 all ratios also as functions of χ .

Although the basic assumption $\chi_\theta = 1$ underlying the model of Wu & Libchaber (1991) and Zhang *et al.* (1997) turns out not to be valid for our experimental data for water, we briefly sketch their derivation of the Nusselt-number modification in the NOB case further. In order to calculate the Nusselt number, Wu & Libchaber (1991) adopt the previous hypothesis by Castaing *et al.* (1989) and assume that the heat flux Q in the center range is determined by the velocity fluctuation u_c and the temperature fluctuations Δ_c only:

$$Q \sim \rho c_p u_c \Delta_c. \quad (5.6)$$

With $u_c \sim \sqrt{g\beta_c \Delta_c L}$ and with furthermore assuming that the BL temperature scale $\theta_t = \theta_b$ is the same as the bulk temperature fluctuation Δ_c , cf. eq. (5.3), together with

$Q = \Lambda_{\bar{t}} \Delta_{\bar{t}} / \lambda_{\bar{t}} = \Lambda_{\bar{b}} \Delta_{\bar{b}} / \lambda_{\bar{b}}$, cf. eq. (5.1), and the notation

$$\left(\frac{\nu \kappa}{\beta} \right)^{1/3} \frac{1}{\Lambda} \equiv S, \quad (5.7)$$

one finally obtains

$$Nu \sim \left(\frac{\nu_m}{\nu_c} \right)^{3/7} \left(\frac{\kappa_m}{\kappa_c} \right)^{-6/7} \left(\frac{\beta_c}{\beta_m} \right)^{2/7} \left(\frac{2S_c}{S_{\bar{t}} + S_{\bar{b}}} \right)^{9/7} Ra_m^{2/7} Pr_m^{-1/7}. \quad (5.8)$$

As in the 1989 Chicago model, one finds the scaling law $Nu \propto Ra^{2/7}$. This scaling law is not globally valid, cf. Grossmann & Lohse (2000, 2001); Xu *et al.* (2000) and many other references. It is nevertheless interesting to consider the change of Nu under NOB effects,

$$\frac{Nu_{NOB}}{Nu_{OB}}|_{WL} = \left(\frac{\nu_m}{\nu_c} \right)^{3/7} \left(\frac{\kappa_m}{\kappa_c} \right)^{-6/7} \left(\frac{\beta_c}{\beta_m} \right)^{2/7} \left(\frac{2S_c}{S_{\bar{t}} + S_{\bar{b}}} \right)^{9/7}. \quad (5.9)$$

Note that the first three factors in eq. (5.9) $F_3 = \left(\frac{\nu_m}{\nu_c} \right)^{3/7}$, $F_4 = \left(\frac{\kappa_m}{\kappa_c} \right)^{-6/7}$, and $F_5 = \left(\frac{\beta_c}{\beta_m} \right)^{2/7}$ only originate from the fact that the Nusselt numbers are given in terms of Ra and Pr at T_m and are nondimensionalised with κ_m . These factors are not used by Wu & Libchaber (1991), as the Rayleigh and Prandtl numbers in the theoretical part of that paper are defined in terms of T_c . Here we use T_m instead of T_c as the reference temperature, because T_m is the external control parameter, while T_c depends on the *a priori* unknown response of the RB flow to NOB conditions and on the material properties at this center temperature.

Although basic assumptions to derive it are not valid, equation (5.9) turns out to describe the measured ratio of the NOB and the OB Nusselt numbers surprisingly well, see Fig. 13. Here we calculated the ratio Nu_{NOB}/Nu_{OB} for water in the medium cell as function of Ra with the help of the experimentally determined function $\chi(Ra)$ (and not of χ_{WL}). Not only is the robustness of Nu with respect to NOB effects correctly reflected, but even the small *decrease* of Nu_{NOB} as compared to Nu_{OB} is given by expression (5.9). This holds in spite of the disagreement between the experimental and theoretical χ ratio and the violation of the basic assumption $\chi_{\theta} = 1$ of the model. We conclude that the value of χ has little effect on the NOB corrections to the Nusselt number, which are robustly very small. A similar conclusion seems to be valid concerning the local Ra -scaling exponent of Nu , since also $2/7$ is not verified experimentally.

Let us look at the Δ -dependences of the individual factors of equation (5.9), F_3 , F_4 , F_5 , and $F_6 = \left(\frac{2S_c}{S_{\bar{t}} + S_{\bar{b}}} \right)^{9/7}$ in more detail; see figure 14. The last factor F_6 again has the property that only the sum of the bottom and the top layer contributions of the quantity S appears. Thus, in lowest, linear order in the temperature deviations also here the NOB effects from the top and bottom BL compensate each other. Indeed, this factor F_6 is nicely described by a *quadratic* dependence on Δ , namely by $F_6 = 1 - 3.07 \cdot 10^{-5} \Delta^2$. The other factors F_i , $i = 3, 4, 5$, however introduce linear dependences on Δ .

Since ratios of bottom and top quantities are of particular interest to characterize deviations from OB conditions quantitatively, $\chi = \chi_{\Delta}$ in particular, but also χ_{κ} , χ_{ν} , χ_{β} (and in the frame of the Wu-Libchaber model also χ_{θ}), we now check also other such ratios. Consider first the Δ or $\Delta/\Delta_{m,medium} = Ra$ dependence of the ratio of the bottom

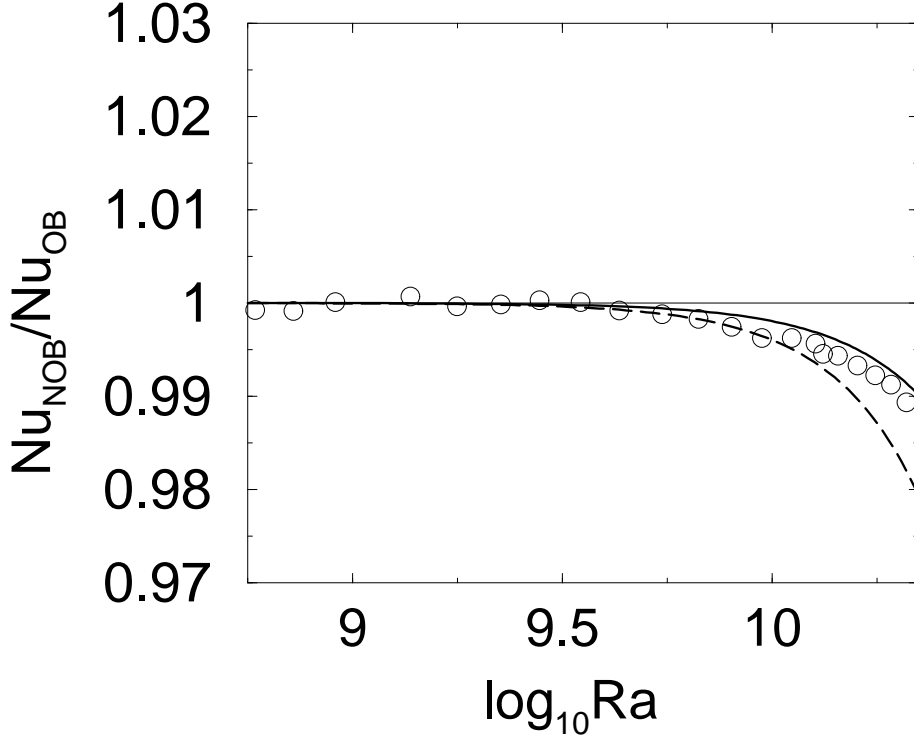


FIGURE 13. Nu_{NOB}/Nu_{OB} versus Ra for water and $T_m = 40^\circ\text{C}$ and $Pr = 4.38$ from our measurements with the medium cell (circles), from the Wu-Libchaber model Eq. (5.9) (dashed line) but with the ratio χ as measured in our water experiments in the medium cell, and from the theory of Sect. 6 (solid line). Note the scale on the ordinate, as compared to the corresponding ordinate scale on the figures for the χ 's: The Nusselt number is very robust to NOB effects.

and top Rayleigh numbers $\chi_{Ra} = Ra_b/Ra_t$, with

$$Ra_b = \frac{g\beta_{\bar{b}}\lambda_{\bar{b}}^3\Delta_b}{\nu_{\bar{b}}\kappa_{\bar{b}}} = \frac{\Delta_b}{\theta_b} \quad (5.10)$$

and Ra_t correspondingly. We have

$$\chi_{Ra} = \frac{Ra_b}{Ra_t} = \chi\chi_{\theta}^{-1}. \quad (5.11)$$

The BL thickness ratio in the Wu-Libchaber approximation is $\chi_{\lambda} = \frac{\lambda_{\bar{b}}}{\lambda_{\bar{t}}} = \frac{\kappa_{\bar{b}}}{\kappa_{\bar{t}}} \chi$. Furthermore, there are various velocity scales in the RB system. Define w_b as that velocity scale in the BL for which buoyancy is of the order of the viscous loss, $g\beta_{\bar{b}}\Delta_b \sim \nu_{\bar{b}}w_b/\lambda_{\bar{b}}^2$, leading to

$$\chi_w = \frac{w_b}{w_t} = \frac{\beta_{\bar{b}}\nu_{\bar{t}}}{\beta_{\bar{t}}\nu_{\bar{b}}} \frac{\Delta_b}{\Delta_t} \left(\frac{\lambda_{\bar{b}}}{\lambda_{\bar{t}}}\right)^2 = \chi_{\beta} \chi_{\nu}^{-1} \chi \chi_{\lambda}^2. \quad (5.12)$$

Also of interest is this velocity scale in the boundary layers. In the bottom BL the relevant length scale is $\lambda_{\bar{b}}$; the relevant temperature difference either is Δ_b or θ_b . Defining thus

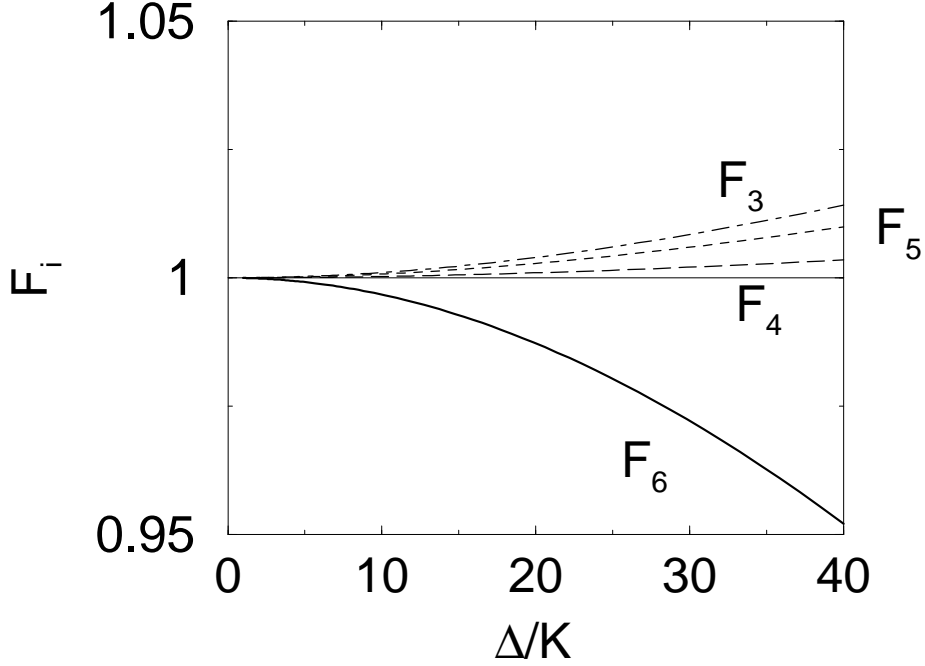


FIGURE 14. The individual factors of eq. (5.9) as functions of Δ for water and $T_m = 40^\circ\text{C}$: $F_3(\Delta)$ (short-long-dashed), $F_4(\Delta)$ (long-dashed), $F_5(\Delta)$ (short-dashed), and $F_6(\Delta)$ (solid). The factor F_6 can be fitted by $F_6 = 1 - 3.07 \cdot 10^{-5} \Delta^2$. This fit is indistinguishable from the curve itself.

$u_b = (\beta_b g \Delta_b \lambda_b)^{1/2}$ and $\tilde{u}_b = (\beta_b g \theta_b \lambda_b)^{1/2} = \left(\frac{\nu_b}{\lambda_b} \frac{\kappa_b}{\lambda_b} \right)^{1/2}$ one is led to

$$\chi_u = \frac{u_b}{u_t} = \left(\frac{\beta_b}{\beta_t} \chi \chi_\lambda \right)^{1/2} \quad (5.13)$$

and

$$\chi_{\tilde{u}} = \frac{\tilde{u}_b}{\tilde{u}_t} = \chi_\nu^{1/2} \chi_\kappa^{1/2} \chi_\lambda^{-1}. \quad (5.14)$$

Note that \tilde{u}_b (and correspondingly \tilde{u}_t) is the geometric mean of the viscous and the thermal molecular velocities in the boundary layer, independent of any buoyancy.

We present various of these ratios for the case of water as working fluid in Figure 11 as functions of Δ and of $\Delta/\Delta_{m,medium} = Ra$. They all show prominent NOB effects. The Ra -ratio χ_{Ra} and also $\chi_{\tilde{u}}$ have only moderate deviations from the OB value $\chi_X = 1$. But apparently they too are not Δ -independent constants. For better comparison with Wu and Libchaber's curves (Wu & Libchaber (1991)) we also present the ratios of interest as functions of the preferred measure for NOB effects, the BL temperature ratio $\chi = \chi_\Delta$ (figure 12).

6. Extension of boundary layer theory to NOB conditions

6.1. Motivation

The previous section has shown the shortcomings of the Wu-Libchaber model in explaining the center temperature T_c and thus χ in the examined water NOB case. In this section

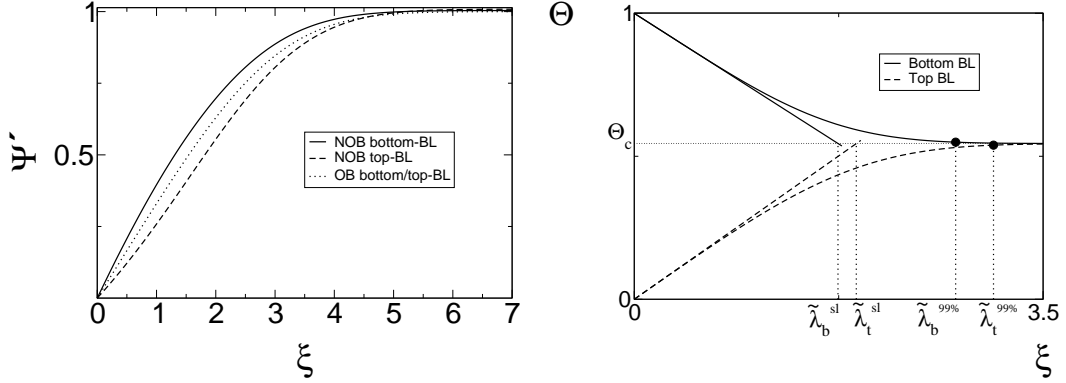


FIGURE 15. (Dimensionless) longitudinal velocity $\Psi' = u_x/U_{NOB}$ (left) and temperature Θ (right) profiles for water at $T_m = 40^\circ C$ and $\Delta = 40^\circ C$ in the NOB-case. The center temperature Θ_c is larger than the mean temperature $\Theta_m = 0.5$. The bottom slope-based thermal BL is smaller than the corresponding one at the top plate, $\lambda_b^{sl} < \lambda_t^{sl}$.

we will present an alternative theory which will not have these shortcomings and which will be able to consistently account for all measured NOB relative to the OB data for water. It is based on the Prandtl-Blasius theory for laminar BLs (Prandtl (1905); Blasius (1908); Pohlhausen (1921); Meksyn (1961); Landau & Lifshitz (1987); Schlichting & Gersten (2000)), extended to temperature dependent viscosity and thermal diffusivity (Plapp (1957)); see also Zhang *et al.* (1997); Wall & Wilson (1997), who considered the case of temperature dependent viscosity only. The justification to start from the Prandtl-Blasius BL theory is that for water even for $Ra = 10^{11}$ the wall Reynolds number is not larger than about 100. Indeed, the Grossmann-Lohse unifying theory of RB convection (Grossmann & Lohse (2000, 2001, 2002, 2004)), which is able to account for the measured $Nu(Ra, Pr)$ and $Re(Ra, Pr)$ in a considerable part of the parameter space, employs the scaling of the Prandtl-Blasius BL theory as a central ingredient, although the layers certainly show plume separation and therefore time dependence. But they are not yet fully turbulent and therefore not fluctuation dominated.

In subsection 2.4 we have already addressed how the BL thicknesses will be modified in the NOB case. We will now calculate the full velocity and temperature profiles and from those derive the center temperature T_c and thus the ratio $\chi = \frac{\Delta_b}{\Delta_t}$ (subsection 6.2), which are found to be in very good agreement with the experimental data. No fitting parameter has to be introduced. When in addition employing the experimental finding of figure 10 that for water the factor F_1 within experimental resolution is $F_1 = 1$ in the Δ -range of interest, meaning that the sum of the top and bottom thermal boundary layer widths (based on the slopes of the temperature profiles at the plates) remains unchanged in the NOB case, the theory also gives the measured small Nusselt number reduction for the NOB case and an at most 0.5% increase in the Reynolds number for the Δ considered here, which is also consistent with the experimental data (subsection 6.3). In subsection 6.4 we explore the origin of the NOB corrections by studying hypothetical liquids with only one of the material parameters being temperature dependent. In subsection 6.5 we apply our theory to glycerol and make predictions for the NOB effects in that liquid.

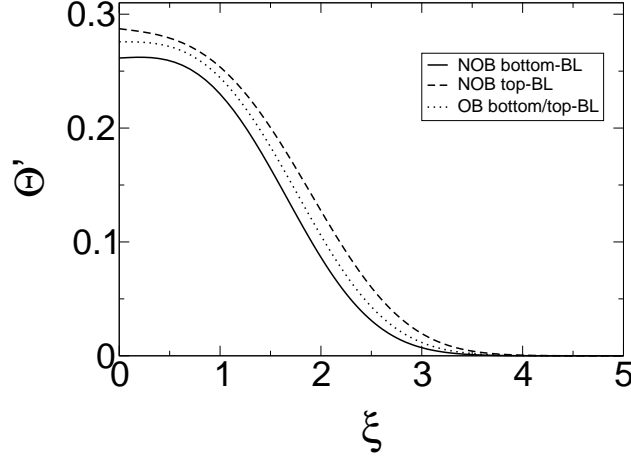


FIGURE 16. (Dimensionless) slope of the temperature profiles in the top and bottom NOB thermal BLs. The same liquid (water) and parameters T_m , and Δ as in figure 15 is chosen.

6.2. Viscous and thermal boundary layers with temperature dependent viscosity and thermal diffusivity

As pointed out in section 2, for water one can assume to a very good approximation that the fluid density and the isobaric specific heat capacity are constant, i.e., throughout equal to ρ_m and $c_{p,m}$, respectively. In contrast, the temperature dependences of the kinematic viscosity $\nu(T) = \eta(T)/\rho_m$, the thermal diffusivity $\kappa(T) = \Lambda(T)/(c_{p,m}\rho_m)$ are explicitly taken into consideration and calculated according to Appendix A.

In this approximation Prandtl's equation, on which Prandtl's stationary BL theory is based, reads

$$u_x \partial_x u_x + u_z \partial_z u_x = \partial_z (\nu \partial_z u_x). \quad (6.1)$$

Pressure contributions are omitted. u_x is the horizontal velocity component at the bottom or top plates in the direction of the large-scale circulation (the wind of turbulence), and u_z is the vertical velocity component. Both velocity components are taken to be uniform in the lateral, y -direction, i.e., in the direction perpendicular to the wind, and are functions of x and z only. The following boundary conditions apply:

$$u_x(x, 0) = 0, \quad (6.2)$$

$$u_z(x, 0) = 0, \quad (6.3)$$

$$u_x(x, \infty) = U_{NOB}. \quad (6.4)$$

The longitudinal asymptotic velocity U_{NOB} outside the viscous BL is identified with the wind of turbulence. Note that U_{NOB} is not necessarily the same as U_{OB} , since it may vary with the bulk properties, in particular with T_c , and thus with Δ . Its value is part of the boundary conditions. For solving the BL equations the only thing which matters is to fix the asymptotic ($z \rightarrow \infty$) value of $u_x(x, z)$. The difference between U_{NOB} and U_{OB} will be determined by an additional input, taken from an argument beyond boundary layer theory, namely, the experimental finding that the sum of the *physical* boundary layer thicknesses for water has been measured as independent of Δ .

Analogously, the thermal boundary layer is described by:

$$u_x \partial_x T + u_z \partial_z T = \partial_z (\kappa \partial_z T), \quad (6.5)$$

with the boundary conditions:

$$T(x, 0) = T_b \text{ or } T(x, 0) = T_t, \quad (6.6)$$

$$T(x, \infty) = T_c. \quad (6.7)$$

The two possible boundary conditions describe two plates facing each other, one being the top plate and the other one the bottom plate. The asymptotic temperature of the fluid outside of each thermal BL is T_c , which under NOB conditions is not the same as T_m . Its value is part of the boundary conditions as well and will be determined by the constraint that the thermal current across the RB container is conserved, as will be explained below.

Now, the temperature is measured as the deviation from the top temperature and is non-dimensionalized† with Δ ,

$$\Theta = \frac{T - T_t}{\Delta} = \frac{T - T_m}{\Delta} + \frac{1}{2}. \quad (6.8)$$

Then $\Theta_m = 1/2$ and the thermal boundary conditions for the bottom and top plates read $\Theta_b = 1$ and $\Theta_t = 0$. The central new element as compared to the standard laminar BL theory is that both the kinematic viscosity and the thermal diffusivity are now temperature dependent – in dimensionless form $\tilde{\nu}(\Theta) = \nu(T)/\nu_m$ and $\tilde{\kappa}(\Theta) = \kappa(T)/\kappa_m$, respectively, giving rise to extra terms when performing the z -derivatives on the right hand sides of eqs. (6.1) and (6.5), respectively.

We now reduce eqs. (6.1) and (6.5) to ODEs by introducing a stream-function ψ and then by employing its self-similarity under x and z changes. A stream-function ψ can be introduced because Prandtl's BL theory deals with two-dimensional, incompressible flow. It satisfies $u_x = \partial_z \psi$ and $u_z = -\partial_x \psi$. In analogy with the OB-case, we introduce the transverse length-scale ℓ_{NOB} :

$$\ell_{NOB} \equiv \sqrt{\frac{x \nu_m}{U_{NOB}}}. \quad (6.9)$$

This length scale is defined in terms of the asymptotic velocity U_{NOB} as the velocity scale, since this choice guarantees that the boundary condition for the stream-function will always be $\Psi'(\infty) = 1$, independent of Δ . As U_{NOB} is a priori unknown, so is ℓ_{NOB} . Next, the similarity variable ξ is introduced,

$$\xi \equiv z \sqrt{\frac{U_{NOB}}{x \nu_m}} = \frac{z}{\ell_{NOB}}. \quad (6.10)$$

The stream function $\psi(x, z)$ is assumed to depend on this (x, z) -combination only, implying a self-similar solution. As in the standard Prandtl theory, ψ is non-dimensionalized as

$$\Psi(\xi) = \frac{\psi(x, z)}{\ell_{NOB} U_{NOB}}. \quad (6.11)$$

With this nondimensional self-similarity ansatz for the stream function one finds from the Prandtl equation (6.1) the ODE

$$\tilde{\nu} \Psi''' + \left(\frac{1}{2} \Psi + \frac{d\tilde{\nu}}{d\Theta} \Theta' \right) \Psi'' = 0. \quad (6.12)$$

† Distinguish Θ from θ , the temperature in K as measured from the chosen reference temperature, usually T_m , introduced already above.

The boundary conditions are

$$\Psi(0) = 0, \quad (6.13)$$

$$\Psi'(0) = 0, \quad (6.14)$$

$$\Psi'(\infty) = 1. \quad (6.15)$$

Note that the velocity profile $\Psi' = u_x/U_{NOB}$ depends explicitly on viscosity and implicitly on the thermal diffusivity (since the Θ profile depends on Pr , as will be shown below, cf. eq.(6.16)). Therefore, the solution of the dimensionless boundary value problem (6.12)-(6.15) is *nonuniversal*. Namely, it depends on the material parameters and their respective temperature dependences.

Correspondingly, from the temperature equation (6.5) one obtains for the similarity function Θ , describing the temperature field $\Theta(x, z) = \Theta(\xi)$

$$\tilde{\kappa} \Theta'' + \left(\frac{1}{2} Pr \Psi + \frac{d\tilde{\kappa}}{d\Theta} \Theta' \right) \Theta' = 0. \quad (6.16)$$

There are two possible boundary conditions, either for the bottom or for the top BL

$$\Theta(0) = \Theta_b = 1 \text{ or } \Theta(0) = \Theta_t = 0, \quad (6.17)$$

$$\Theta(\infty) = \Theta_c. \quad (6.18)$$

Thus in the RB configuration, each thermal plate is associated with a boundary layer described by (6.12)-(6.15) coupled to (6.16)-(6.18). Therefore, in principle, it would be just a matter of integrating the top and bottom BL-equations, as done in the OB-case. However, the NOB-case has a subtle point: the asymptotic temperature $\Theta_c = \frac{T_c - T_t}{\Delta}$, with $0 < \Theta_c < 1$, is a *response* parameter, which has not been fixed yet. Therefore, in order to solve the BL equations, one has first to identify the centre (bulk) temperature T_c and thus the boundary-condition (6.18).

We determine Θ_c by the constraint that the thermal flux across the cell is conserved and therefore the influx at the bottom must be the same as the outflux at the top, $J(z=0) = J(z=L)$. This means

$$\kappa_b \partial_z T|_b = \kappa_t \partial_z T|_t \quad (6.19)$$

or in dimensionless form

$$\tilde{\kappa}_b |\Theta'_b| = \tilde{\kappa}_t \Theta'_t. \quad (6.20)$$

This determines the bulk temperature Θ_c .

The BL equations (6.12)-(6.15) and (6.16)-(6.18) are iteratively solved until condition (6.20) is satisfied. Technically, this can e.g. be achieved with a shooting method (cf. Press *et al.* (1986)). The solution gives the center temperature T_c (shown in figure 5), or alternatively the temperature drops Δ_t and Δ_b (shown in figure 4) over the top and bottom thermal BLs and of course their ratio χ (shown in figure 6). All these theoretical results are in good agreement with our measurements. We stress that the computation is based on two ingredients only: (i) the dimensionless BL-equations, (6.12)-(6.15) and (6.16)-(6.18), assisted by the given temperature dependences of the fluid properties and (ii) the conservation of the thermal current. No additional input or fitting parameter is needed.

The solution of the BL equations also gives the dimensionless velocity and temperature profiles, see figure 15. Both the kinetic and the thermal bottom BLs are thinner than the respective top BLs, as already argued in section 2 for the thermal BLs. In the right panel of figure 15 the difference in the slope-based thermal BL thicknesses λ_b^{sl} and λ_t^{sl}

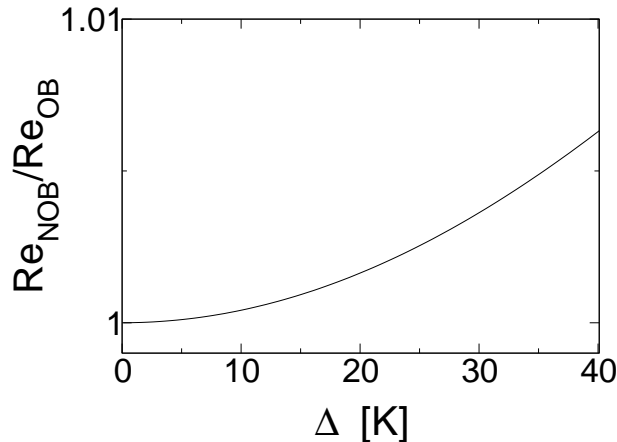


FIGURE 17. Re_{NOB}/Re_{OB} versus Δ for the medium cell with $T_m = 40^\circ\text{C}$ and $Pr = 4.38$ from the theory of section 6. Note the scale of the ordinate, as compared to the ordinate scale in the figures for the χ 's: Also the Reynolds number is very robust towards NOB corrections. Due to the deviations from the OB conditions the wind amplitude slightly increases, while the heat current was found to slightly decrease.

is explicitly shown. It is also seen that Θ_c is larger than $\Theta_m = 1/2$. All NOB profiles are characterized by a pronounced curvature, as also already qualitatively discussed in section 2. Figure 16 shows the moduli of the dimensionless temperature slopes Θ' : They are different at the top and bottom plates and vary strongly with height (z), due to the temperature dependence of the thermal diffusion coefficient.

The temperature and velocity profiles remain to be measured. Note that the theory can only predict the *shape* of the profile including its nondimensional thickness, but not its absolute, physical thickness, since the yet unknown velocity U_{NOB} (and derived from this the unknown transverse length-scale ℓ_{NOB}) is involved in the nondimensionalization.

6.3. Application of NOB boundary layer theory to Nu and Re

The lack of knowledge of U_{NOB} (and thus of ℓ_{NOB}) also is the reason why the Nusselt number Nu_{NOB} cannot yet be calculated. This is of course not surprising as the considered BL theory does not take notice of the thermal expansion coefficient β , which is responsible for the buoyant driving of the flow. We have calculated, instead, the change of Nu_{NOB} relative to Nu_{OB} due to the NOB influences. The relevant formulas are eqs. (4.1),(4.2),(4.3). While F_2 can be calculated from the nondimensionalized BL theory immediately, because only nondimensional NOB quantities enter, the ratio of the sum of the BL thicknesses $F_1 = 2\lambda_{OB}^{sl}/(\lambda_t^{sl} + \lambda_b^{sl})$, cf. eq. (4.2), contains the length ratio $\ell_{OB}/\ell_{NOB} = \sqrt{U_{NOB}/U_{OB}}$. Since the velocities U_{NOB} , U_{OB} feel the buoyancy in the bulk, they are expected to be influenced by the NOB-changes of the thermal expansion coefficient from β_m to β_c .

In order to determine the ratio U_{NOB}/U_{OB} we consider the thickness ratio F_1 , see eq.(4.2). From our experiments in water we know that in this liquid within experimental resolution we have $F_1 = 1$, i.e., the sum of the physical top and bottom thermal BL thicknesses remains constant under deviations from OB conditions, see figure 10 in section 4. Therefore we can use F_1 , here $F_1 = 1$, as an additional ingredient from experiment to be able to calculate Nu_{NOB}/Nu_{OB} within the extended BL theory.

Write F_1 in terms of the dimensionless thicknesses and the respective length scales,

$$F_1 = \frac{2 \tilde{\lambda}_{OB}^{sl} \ell_{OB}}{\tilde{\lambda}_t^{sl} + \tilde{\lambda}_b^{sl} \ell_{NOB}} = \tilde{F}_1 \sqrt{\frac{U_{NOB}}{U_{OB}}}. \quad (6.21)$$

Then one has

$$\frac{U_{NOB}}{U_{OB}} = \frac{Re_{NOB}}{Re_{OB}} = \left(\frac{F_1}{\tilde{F}_1} \right)^2. \quad (6.22)$$

The nondimensional factor $\tilde{F}_1 = 2 \tilde{\lambda}_{OB}^{sl} / (\tilde{\lambda}_t^{sl} + \tilde{\lambda}_b^{sl})$ is fully provided by the Prandtl-Blasius boundary layer theory, namely by the integration of (6.12)-(6.15) together with (6.16)-(6.18). F_1 is taken as an input from experiment, here $F_1 = 1$. Then eq.(6.22) determines the U or Re ratio.

With the same experimental input of F_1 (in particular $F_1 = 1$ for the water case), the Nusselt number ratio follows from the exact relation (4.1),

$$\frac{Nu_{NOB}}{Nu_{OB}} = \frac{2 \lambda_{OB}^{sl}}{\lambda_t^{sl} + \lambda_b^{sl}} \cdot \frac{\kappa_t \Delta_t + \kappa_b \Delta_b}{\kappa_m \Delta} = F_1 \cdot F_2 = F_2 = \frac{\kappa_t \Delta_t + \kappa_b \Delta_b}{\kappa_m \Delta}, \quad (6.23)$$

i.e., directly from the results for Δ_t and Δ_b of the previous subsection. The resulting dependence of the heat flux ratio on Δ or on $Ra = \frac{\beta_m g L^3}{\nu_m \kappa_m} \Delta$ was shown in figure 13, together with the experimental data. Very good agreement is seen. Not only the robustness of the Nusselt number towards NOB corrections is found, but even the tiny 1% decrease of Nu_{NOB} as compared to Nu_{OB} . The Reynolds number ratio $Re_{NOB}/Re_{OB} \propto \tilde{F}_1^{-2}$, cf. eq. (6.22), is shown in figure 17. Also the Reynolds number turns out to be very robust towards NOB corrections. It increases by about 0.5% as compared to the OB case. This theoretical finding also is consistent with our measurements (cf. figure 8), showing less than 2% variation of Re_{NOB} (which is our experimental error bar) due to NOB effects.

6.4. Origin of NOB corrections for χ and Nu

In order to shed light on the origin of the various features of the NOB corrections, the Nu robustness in particular, we now consider the NOB corrections for hypothetical liquids with (i) $\nu(T)$ as in water, but $\kappa = \kappa_m$ being constant and (ii) $\kappa(T)$ as in water, but $\nu = \nu_m$ being constant. The results for χ are shown in figure 18. For the ratios Nu_{NOB}/Nu_{OB} and Re_{NOB}/Re_{OB} as displayed in figure 19 we in addition assume that $F_1 = 1$ also for the hypothetical liquids. Note that Δ_b , Δ_t , χ , and F_2 can be calculated from the BL theory without any fit parameter and without any measured data, using only theory and the given material properties. But in order to determine the Nu - and Re -ratios, we again have to know F_1 . Although obviously F_1 cannot be measured for hypothetical liquids, we still assume $F_1 = 1$ as an extra hypothesis. These calculations with hypothetical liquids quantify our qualitative discussions of section 4.

From the figures we conclude that T_c and thus Δ_b , Δ_t , and χ are mainly determined by the temperature dependence of the viscosity $\nu(T)$. The variation of the thermal diffusivity $\kappa(T)$ with T has only a small influence on these quantities. In contrast, within our theory the Nusselt number modification under NOB effects is exclusively determined by the temperature dependence of $\kappa(T)$. As can be seen easily from eq. (4.1), a temperature dependence of the viscosity $\nu(T)$ but with $\kappa = \kappa_m$ being constant, has no effect on the Nusselt number, in spite of the modification of the central temperature (remember always that $F_1 = 1$ is assumed).

The physical reason that Nu and Re are so robust under large changes of the material parameters with the temperature is that F_2 does not take notice of the linear, dominant variations of κ, ν , etc. F_2 is affected only by the higher order, nonlinear changes of the

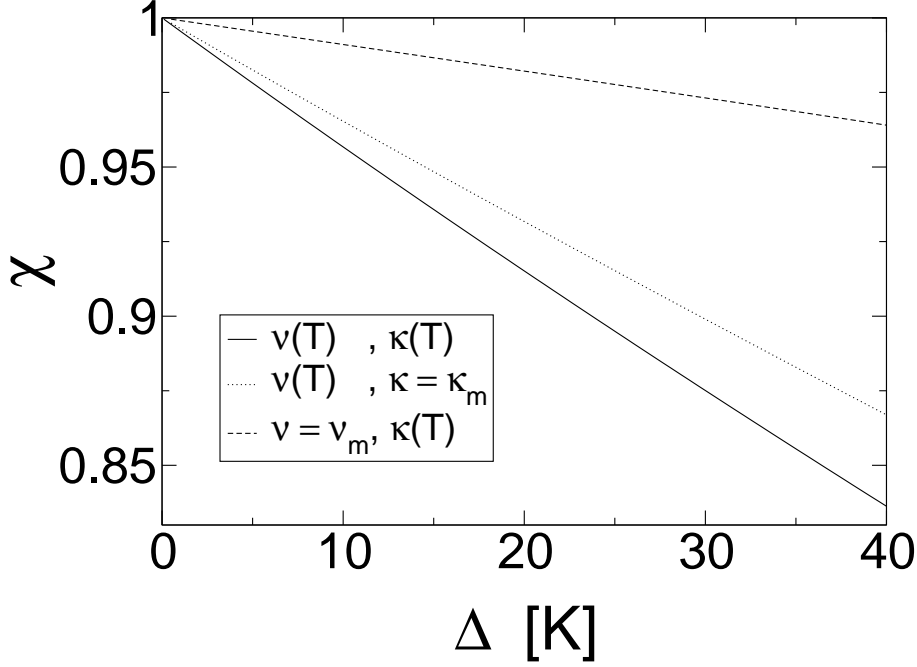


FIGURE 18. $\chi = \Delta_b/\Delta_t$ versus Δ for the medium cell with $T_m = 40^\circ\text{C}$, but filled with hypothetical liquids. The solid line takes the full temperature dependence of both $\nu(T)$ and $\kappa(T)$ into consideration, i.e., represents real water. The dotted line shows χ for a hypothetical liquid with $\nu(T)$ as in water, but κ_m being constant. Vice versa, the dashed line shows the ratio χ for a hypothetical liquid with $\kappa(T)$ as in water, but ν_m being constant. Only the extended Prandtl-Blasius BL theory is used, no further experimental input.

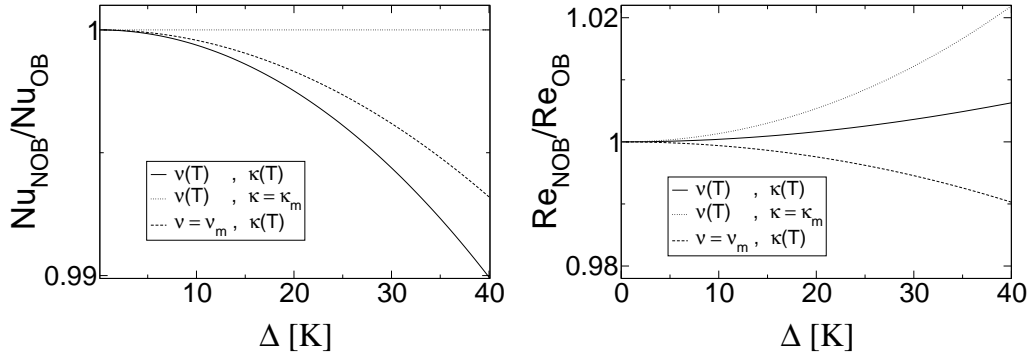


FIGURE 19. Nu_{NOB}/Nu_{OB} (left) and Re_{NOB}/Re_{OB} (right) versus Δ for the medium cell with $T_m = 40^\circ\text{C}$, filled with either water (solid lines) or with hypothetical liquids (dashed or dotted lines). The solid lines are valid if the temperature dependence of both $\nu(T)$ and $\kappa(T)$ as in water is taken into account. The dotted lines show the Nusselt and Reynolds number changes for a hypothetical liquid with $\nu(T)$ as in water, but κ_m being constant. Vice versa, the dashed lines show these numbers for a hypothetical liquid with $\kappa(T)$ as in water, but ν_m being constant. For comparison the value $F_1 = 1$ for the factor describing the OB/NOB boundary layer thickness ratio is used also for the hypothetical liquids.

material parameters. These are visible as curvatures (or even the changes of those) of $(\kappa(T) - \kappa_m)/\kappa_m$, $(\nu(T) - \nu_m)/\nu_m$, etc., as seen in Figure 22. The dominant, linear contributions in the material parameters cancel by the shift of the bulk temperature $T_m \rightarrow T_c$.

To understand this cancellation of the bottom and top NOB effects in linear ($\propto \Delta$) order even analytically as far as F_2 is concerned, we apply a systematic expansion of the involved quantities in terms of Δ . We have from Figure 5, caption, that $(T_c - T_m)/\Delta = c_2\Delta + c_3\Delta^2 + c_4\Delta^3$ and from the appendix, eq. (A 1) the expansions $\kappa_{b,t}/\kappa_m = 1 \pm a_{\kappa,1}\Delta/2 + a_{\kappa,2}\Delta^2/4 \pm a_{\kappa,3}\Delta^3/8$; here \pm corresponds to b, t (bottom, top). This leads to

$$F_2(\Delta) = 1 + d_2\Delta^2 + d_3\Delta^3 + d_4\Delta^4 . \quad (6.24)$$

One easily convinces oneself that the linear terms $\propto \Delta$ cancel. The deviation from $F_2 = 1$ starts with Δ^2 . Between the contributing coefficients the following relations are valid.

$$d_2 = \frac{a_{\kappa,2}}{4} - a_{\kappa,1} c_2 \quad , \quad d_3 = -a_{\kappa,1} c_3 \quad , \quad d_4 = -(a_{\kappa,1} c_4 + a_{\kappa,3} c_2) . \quad (6.25)$$

With the numerical values for the $a_{\kappa,i}$ from table 2 and for the c_j from the caption of Figure 5 one obtains $d_2 = -7.2 \times 10^{-6} K^{-2}$, in good agreement to what had been found from the data for F_2 , see inset of Figure 10. Both terms in the sum for d_2 , the quadratic order κ -coefficient as well as the product of the linear order κ - times the linear order $\frac{T_c - T_m}{\Delta}$ -contribution are negative and amplify their effects. For the next coefficient one calculates $d_3 = 3.2 \times 10^{-8} K^{-3}$. The fourth order term d_4 consists of the first term only, since according to table 2 one has $a_{\kappa,3} = 0$. This gives $d_4 = -3.2 \times 10^{-10} K^{-4}$. Equations (6.24) and (6.25) give a consistent analytical description of the thermal NOB effects, connecting $\kappa(T)$ with T_c . All these statements also hold for Nu_{NOB}/Nu_{OB} , as long as $F_1 = 1$, as we have measured for water in the temperature range under investigation.

The quadratic dependence of F_2 on Δ is in agreement with experiment (see figure 10) and has been discussed in section 4. We now also understand what sets the *direction* of the NOB correction to the Nusselt number (provided $F_1 = 1$): It is the sign of the sum constituting $d_2 = -a_{\kappa,1} c_2 + a_{\kappa,2}/4$. The factor $a_{\kappa,1}$ results from the temperature dependence of the thermal diffusivity, while the factor c_2 in addition strongly depends on the temperature dependence of the viscosity $\nu(T)$; it immediately reflects whether T_c is larger than T_m (as for water) or smaller. Furthermore, the curvature coefficient $a_{\kappa,2}$ of the thermal diffusivity $\kappa(T)$ contributes to the sign of the deviation $T_c - T_m$. For water both terms in the sum are negative, thus add to the down shift of Nu_{NOB}/Nu_{OB} . As emphasized already, the effect is quadratic in Δ . The linear contributions from the top and the bottom BL cancel.

The NOB modifications on the Reynolds number Re are more subtle, see figure 19, right. For water, the NOB effects of a temperature dependent viscosity with a constant thermal diffusivity (resulting in a slight enhancement of Re) and those of a temperature dependent thermal diffusivity with a constant viscosity (resulting in a slight decrease of Re) partly compensate each other, leading to only a tiny net enhancement of Re . The reason for the enhanced Reynolds number for the case $\nu(T)$, $\kappa = \kappa_m$ is the overall temperature increase in the cell, $T_c > T_m$, resulting in a smaller cell-averaged viscosity. Note again that according to our theory this does not have any effect on the Nusselt number. The reason for the reduced Reynolds number for the case $\kappa(T)$, $\nu = \nu_m$ is less obvious. Technically, it results from $\tilde{F}_1 > 1$, i.e., $2\tilde{\lambda}_{OB}^{sl} > \tilde{\lambda}_t^{sl} + \tilde{\lambda}_b^{sl}$. But remember that for this discussion we have always made the assumption $F_1 = 1$.

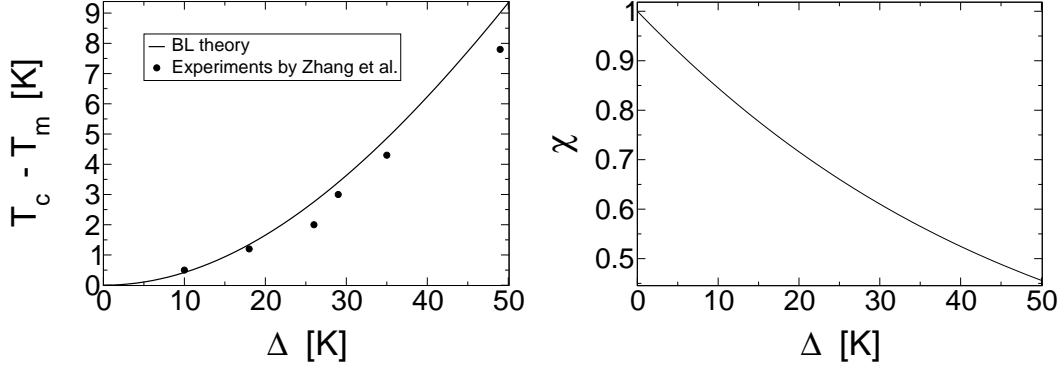


FIGURE 20. (a) The temperature shift in the center of the cylinder filled with glycerol at $T_m = 40^\circ\text{C}$ as a function of Δ . Some experimental values measured by Zhang *et al.* (1997) are also displayed, although for them constant T_m is not valid. Thus the data can only serve for an approximate comparison. This still is reasonably promising. (b) The ratio $\chi = \Delta_b/\Delta_t$ as a function of Δ for glycerol; $T_m = 40^\circ\text{C}$. Note that $T_c - T_m$ is much larger (about 6.5 K) in glycerol than in water (about 1.8 K), both for $\Delta = 40\text{ K}$. The temperature drop ratio χ for glycerol varies by about 50%.

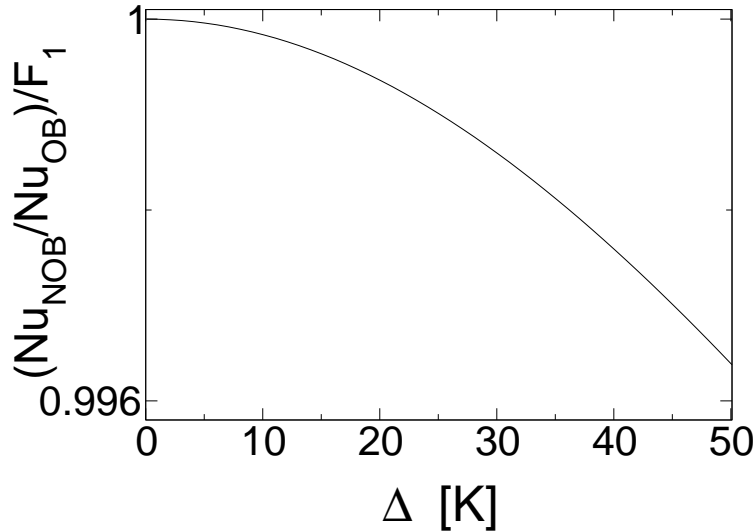


FIGURE 21. The change of the Nusselt number for glycerol under NOB effects. Since no experimental information on the ratio of the total boundary layer thicknesses $F_1 = 2\lambda_{OB}^{sl}/(\lambda_b^{sl} + \lambda_t^{sl})$ is available, we have plotted the Nusselt number divided by F_1 , i.e., the factor F_2 . If we assume that $F_1 \approx 1$ as in water, then the NOB shift in the Nusselt number will be tiny, as anticipated from the hypothetical liquid with temperature dependent $\nu(T)$ while κ is (for glycerol only nearly) constant.

6.5. NOB effects in glycerol

We now theoretically consider NOB effects for another liquid besides of water, namely for glycerol. The reason is to have an independent test for our theory, as there are data for $T_c - T_m$ available from Zhang *et al.* (1997). In that work also Nusselt numbers are

offered, but not the ratio Nu_{NOB}/Nu_{OB} . The glycerol case is a particularly interesting one, because this liquid shows a dramatic change of viscosity $\nu(T)$ with temperature, while the T -dependence of the thermal diffusivity $\kappa(T)$ is rather weak. Thus glycerol is a liquid that approximately behaves like one of the hypothetical liquids studied in the previous subsection.

In the RB cell of Zhang *et al.* (1997), the mean operating temperature for glycerol is sometimes near $T_m = 40^\circ\text{C}$ but is not kept fixed as in our measurements. With $\Delta = 10\text{ K}$ and their cell height $L = 18.3\text{ cm}$ (cubic box, so $\Gamma = 1$) the Rayleigh number is $Ra = 1.29 \times 10^7$. The temperature dependences of the material properties for glycerol are known and can be found in appendix A, table 3. As we have detailed above, within our BL theory the knowledge of the temperature dependent viscosity $\nu(T)$ and thermal diffusivity $\kappa(T)$ is enough to calculate the shift of the center temperature $T_c - T_m$ as a function of Δ , without any fit parameter. Our result is shown in figure 20 and compared with the measured data from Zhang *et al.* (1997). Indeed, our theory is able to reasonably describe the considerable temperature deviation of T_c from T_m also for this case. Fig. 20b shows the corresponding temperature drop ratio $\chi = \Delta_b/\Delta_t$. The increase in T_c as compared to T_m and therefore the deviation from $\chi = 1$ is much more pronounced than for water, shown in Fig. 6. Instead of $\chi = 0.83$ for water we find $\chi = 0.52$ for glycerol, both for $\Delta = 40\text{K}$. Apparently the deviations from linearity are also stronger than for the water case in Fig. 6.

We finally present the Nusselt number ratio under *NOB* in terms of F_1 in Fig. 21. Note that F_1 is still unknown for glycerol. If also for glycerol the conservation of the sum of thicknesses of the thermal BLs under *NOB* deviations held, $F_1 = 1$, the plot would show the Nusselt number ratio directly. For a temperature difference $\Delta = 40\text{K}$ the relative shift is less than about 0.3%, even much less than for water. This is in agreement with the small temperature dependence of $\kappa(T)$, which leads to a factor $F_2 = \frac{\kappa_t}{\kappa_m} \frac{\Delta_t}{\Delta} + \frac{\kappa_b}{\kappa_m} \frac{\Delta_b}{\Delta} \approx 1$.

Clearly, it is of high interest to measure the Nu shift under *NOB* conditions also in glycerol, in order to confirm whether the BL layer thickness sum rule holds. With the then available function F_1 also the Reynolds number modification, Re_{NOB}/Re_{OB} , follows. Both will shed light on the respective roles of the temperature dependence of viscosity $\nu(T)$ and thermal diffusivity $\kappa(T)$. Also the nontrivial validity of the extended Prandtl-Blasius BL theory for the *NOB* case could be confirmed.

7. Summary and conclusions

We have measured *NOB* effects on the ratio χ of the bottom and top temperature drops across the thermal BLs and on the Nusselt number Nu and the Reynolds number Re for turbulent Rayleigh-Bénard convection in water. While χ can vary considerably (up to 20% in the considered case), the *NOB* effects on Nu and Re are very small, resulting in only a less than 2% reduction of Nu and no modification of Re within experimental accuracy (which for Re -measurements is about 2%). This holds even though the viscosity and the thermal expansion coefficient vary by more than a factor of two between the top and bottom plates. We have theoretically accounted for this robustness of Nu and Re towards *NOB* effects: The *NOB* corrections from the top and bottom BLs compensate each other in first order by properly shifting the center temperature $T_m \rightarrow T_c$. We believe that this conclusion is valid beyond the assumptions of constant c_p and ρ . We also expect that it will hold more generally than for water at least for all systems with Pr larger than 1. Then always the thermal boundary layers are nested into the kinetic ones. The robustness of the Nusselt number against *NOB* effects because of the cancellations will thus hold more generally. We have also shown that one of the basic assumptions of the

NOB model by Wu & Libchaber (1991) and Zhang *et al.* (1997) is in conflict with the experimental data. Nonetheless, also that model shows the robustness of Nu towards NOB effects.

An interesting, unexpected and nontrivial finding for water as the working liquid is the observation, that in the considered temperature range the sum of the slope based BL thicknesses $\lambda_b^{sl} + \lambda_t^{sl}$ seems to be invariant under deviations from OB conditions. Within experimental precision it turned out to be constant for even strong NOB effects. The ratio of the NOB and OB heat fluxes Q_{NOB}/Q_{OB} can then be calculated on the basis of the thermal diffusivities κ_b and κ_t at bottom and top and on that of the measured or theoretically evaluated (BL theory) temperature drops Δ_b and Δ_t , cf. eq. (4.6). This ratio is of second order in Δ and thus in NOB effects.

The employed theory is based on the Prandtl-Blasius theory for laminar BLs, extended to temperature dependent viscosity and thermal diffusivity. Remarkably, we do not have to make any use of the temperature dependence of the thermal expansion coefficient. The theory gives a center temperature T_c in very good agreement with the experimental data, without employing any free parameter. With the experimental finding that for water the sum of the slope based thermal BL thicknesses seems to be invariant under deviations from OB, the theory also gives Nusselt and Reynolds number modifications consistent with the measurements. The theory offers the opportunity to discuss hypothetical liquids with only *one* material parameter being temperature dependent, thus shedding light on the mechanism of the NOB corrections: Whereas the NOB correction on χ mainly originates from the temperature dependence of the viscosity, the NOB correction on the Nusselt number exclusively (if $F_1 = 1$) originates from the temperature dependence of the thermal diffusivity.

To further validate our theory, a next step would be to extend the experiments on Rayleigh-Bénard flow under NOB conditions to other liquids, such as e.g. glycerol.

An exciting extension would be to analyse NOB effects also for gases, in particular for those close to the critical point. Then one may have to take Schwarzschild corrections into consideration. Here an interesting case is when the mean temperature is above the critical temperature and the mean density corresponds to the critical value. In that case, the top and bottom boundary layers are nearly symmetric, but nonetheless the fluid properties can vary significantly within them (Oh *et al.* (2004)). These interesting problems go beyond the scope of the present paper. From a theoretical point of view the challenge in the analysis of NOB effects in gases lies in the temperature dependences of the density and the specific heat capacity, which can be and have been considered as constants in the present paper.

The role of the Grossmann-Lohse theory in the present context is to give $Nu(Ra, Pr)$ and $Re(Ra, Pr)$, as long as Δ is small enough to allow neglecting NOB effects. We have seen that in experiment Δ needs not be too small for OB conditions to hold due to the small effects of deviations from OB conditions, the corrections increasing only $\propto \Delta^2$. While in the present paper the BL effects have been dealt with, an extension of GL theory allows to *calculate* also Nu_{NOB} and Re_{NOB} immediately, without further input from experiment. This extended GL theory will be addressed separately. It in particular takes the T -dependence of the expansion coefficient $\beta(T)$ into account explicitly.

Acknowledgement: This work was initiated at the Lorentz-Center Workshop on turbulent thermal convection in Leiden in June 2004 and we would like to express our gratitude to Wim van Saarloos for making such workshops possible. We thank Alexei Nikolaenko for his contributions to the experiments and Enrico Calzavarini and Kazuyasu Sugiyama for discussion. The work in Twente is part of the research program of FOM, which is

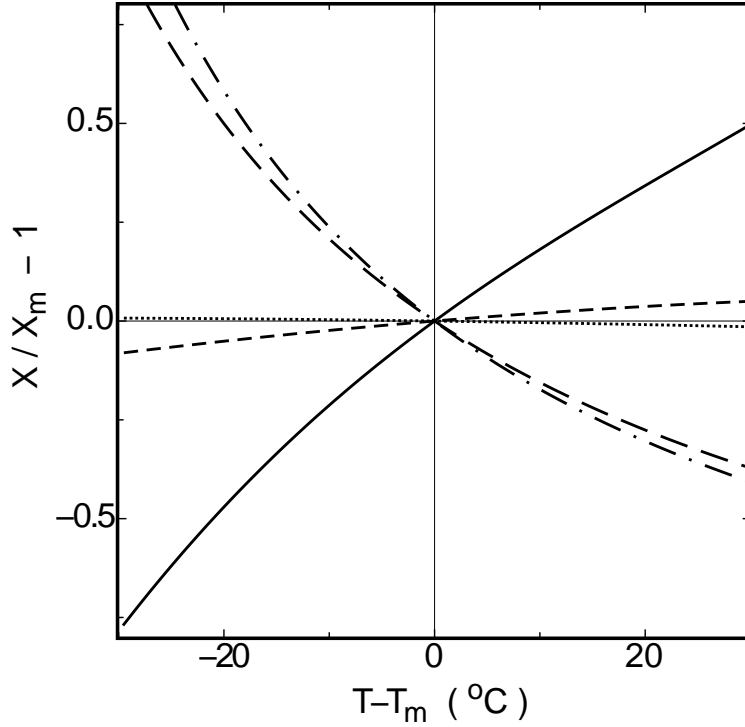


FIGURE 22. The relative deviations $(X - X_m)/X_m$ of water properties X from their values X_m at T_m for $T_m = 40^\circ\text{C}$. Solid line: isobaric thermal expansion coefficient β . Long dashed line: kinematic viscosity ν . Short dashed line: thermal conductivity λ . Dash-dotted line: Prandtl number Pr . Dotted line: density ρ .

financially supported by NWO, and it was also supported (for DL and SGn) by the European Union (EU) under contract HPRN-CT-2000-00162. The work at Santa Barbara was supported by the U.S. Department of Energy through Grant DE-FG02-03ER46080.

Appendix A. Physical properties of water and glycerol

The relative deviations $(X - X_m)/X_m$ from their values X_m at $T_m = 40^\circ\text{C}$ of various physical properties X of water at a pressure of one bar are shown in Fig. 22. One sees immediately that the properties with significant temperature dependences are the thermal expansion coefficient β and the kinematic viscosity ν . The cubic polynomial

$$\frac{X - X_m}{X_m} = a_1(T - T_m) + a_2(T - T_m)^2 + a_3(T - T_m)^3 \quad (\text{A } 1)$$

gave a good fit to the data for each property. In some cases a cubic term was not even needed. The coefficients as well as the values of X_m for $T_m = 40^\circ\text{C}$ are given in Table 2.

For the glycerol case, the dramatic change of viscosity with temperature (as shown in Fig. 23) required a fifth-order polynomial

$$\frac{X - X_m}{X_m} = a_1(T - T_m) + a_2(T - T_m)^2 + a_3(T - T_m)^3 + a_4(T - T_m)^4 + a_5(T - T_m)^5. \quad (\text{A } 2)$$

The coefficients as well as the values of X_m for $T_m = 40^\circ\text{C}$ are given in Table 3.

X	X_m	a_1 $10^{-4} K^{-1}$	a_2 $10^{-6} K^{-2}$	a_3 $10^{-8} K^{-3}$
$\rho/10^3 kg m^{-3}$	0.9922	-3.736	-3.98	-
$c_p/10^3 J kg^{-1} K^{-1}$	4.1690	0.084	4.60	-
$\beta/10^{-4} K^{-1}$	3.8810	195.0	-159.8	207
$\Lambda/W m^{-1} K^{-1}$	0.6297	21.99	-17.8	-
$\kappa/10^{-6} m^2 s^{-1}$	0.1528	23.52	-14.9	-
$\nu/10^{-6} m^2 s^{-1}$	0.6690	-175.9	295.8	-460
Pr	4.3820	-197.6	370	-618

TABLE 2. The values of X_m at $T_m = 40^\circ C$ of several properties X of water and the coefficients obtained by fitting the polynomial eq. (A 1) to data over the range $10 < T < 70^\circ C$.

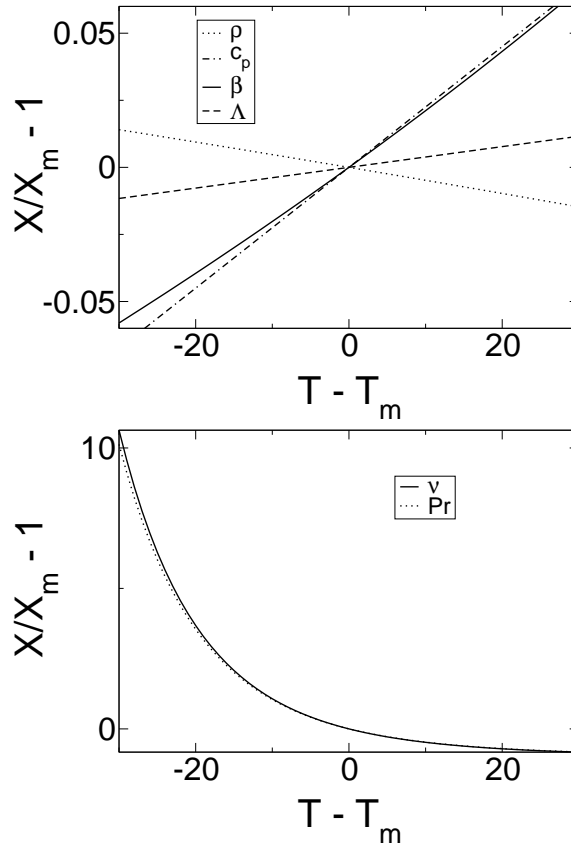


FIGURE 23. The relative deviations $(X - X_m)/X_m$ of glycerol properties X from their values X_m at T_m for $T_m = 40^\circ C$. Upper plate: Solid line: isobaric thermal expansion coefficient β . Short dashed line: thermal conductivity Λ . Dotted line: density ρ . Double-dashed dotted line: specific heat capacity c_p . Lower plate: Solid line: kinematic viscosity ν . Dotted line: Prandtl number Pr . Note the very different scales in the upper and lower plates.

X	X_m	a_1 $10^{-4}K^{-1}$	a_2 $10^{-6}K^{-2}$	a_3 $10^{-8}K^{-3}$	a_4 $10^{-10}K^{-4}$	a_5 $10^{-12}K^{-5}$
$\rho/10^3 kg m^{-3}$	1.2477	-4.789	-0.3795	—	—	—
$c_p/10^3 J kg^{-1}K^{-1}$	2.5108	22.511	—	—	—	—
$\beta/10^{-4}K^{-1}$	4.7893	20.639	4.664	1.0757	0.2540	—
$\Lambda/10^{-3}Wm^{-1}K^{-1}$	2.9351	3.863	—	—	—	—
$\kappa/10^{-6}m^2s^{-1}$	0.0937	13.858	3.913	-0.7577	—	—
$\nu/10^{-6}m^2s^{-1}$	238.71	-702.83	2,393.1	-6,923.0	33,131.3	-71,517.5
Pr	2,547.9	-687.68	2,325.9	-6,646.3	30,875.9	-65,996.9

TABLE 3. The values of X_m at $T_m = 40^\circ C$ of several properties X of glycerol and the coefficients obtained by fitting the polynomial eq. (A 2) to data over the range $10 < T < 70^\circ C$.

REFERENCES

- AHLERS, G. 1980 Effect of departures from the Oberbeck-Boussinesq approximation on the heat transport of horizontal convecting fluid layers. *J. Fluid Mech.* **98**, 137–148.
- AHLERS, G. 2000 Effect of sidewall conductance on heat-transport measurements for turbulent Rayleigh-Bénard convection. *Phys. Rev. E* **63**, 015303.
- ASHKENAZI, S. & STEINBERG, V. 1999 High Rayleigh number turbulent convection in a gas near the gas-liquid critical point. *Phys. Rev. Lett.* **83**, 3641–3644.
- BLASIUS, H. 1908 Grenzschichten in Flüssigkeiten mit kleiner Reibung. *Z. Math. Phys.* **56**, 1–37.
- BODENSCHATZ, E., DEBRUYN, J., AHLERS, G. & CANNELL, D. 1991 Transition between patterns in thermal convection. *Phys. Rev. Lett.* **67**, 3078–3081.
- BODENSCHATZ, E., PESCH, W. & AHLERS, G. 2000 Recent developments in Rayleigh-Bénard convection. *Ann. Rev. Fluid Mech.* **32**, 709–778.
- BOUSSINESQ, J. 1903 *Theorie analytique de la chaleur, Vol. 2*. Paris: Gauthier-Villars.
- BROWN, E., FUNFSCHILLING, D., NIKOLAENKO, A., & AHLERS, G. 2006 Reynolds numbers of the large-scale flow in turbulent Rayleigh-Bénard convection. *unpublished*.
- BROWN, E., FUNFSCHILLING, D., NIKOLAENKO, A. & AHLERS, G. 2005 Heat transport by turbulent Rayleigh-Bénard convection: Effect of finite top- and bottom conductivity. *Phys. Fluids* **17**, 075108.
- BUSSE, F. H. 1967 The stability of finite amplitude cellular convection and its relation to an extremum principle. *J. Fluid Mech.* **30**, 625–649.
- CASTAING, B., GUNARATNE, G., HESLOT, F., KADANOFF, L., LIBCHABER, A., THOMAE, S., WU, X. Z., ZALESKI, S. & ZANETTI, G. 1989 Scaling of hard thermal turbulence in Rayleigh-Bénard convection. *J. Fluid Mech.* **204**, 1–30.
- CHAUMAT, S., CASTAING, B. & CHILLA, F. 2002 Rayleigh-Bénard cells: influence of plate properties. In *Advances in Turbulence IX* (ed. I. P. Castro & P. E. Hancock), Barcelona: International Center for Numerical Methods in Engineering, CIMNE.
- CHAVANNE, X., CHILLA, F., CASTAING, B., HEBRAL, B., CHABAUD, B. & CHAUSSY, J. 1997 Observation of the ultimate regime in Rayleigh-Bénard convection. *Phys. Rev. Lett.* **79**, 3648–3651.
- CHAVANNE, X., CHILLA, F., CHABAUD, B., CASTAING, B. & HEBRAL, B. 2001 Turbulent Rayleigh-Bénard convection in gaseous and liquid he. *Phys. Fluids* **13**, 1300–1320.
- CHILLÀ, F., RASTELLO, M., CHAUMAT, S. & CASTAING, B. 2004 Long relaxation times and tilt sensitivity in Rayleigh-Bénard turbulence. *Euro. Phys. J. B* **40**, 223–227.
- CILIBERTO, S., PAMPALONI, E. & PEREZ-GARCIA, C. 1988 Competition between different symmetries in convective patterns. *Phys. Rev. Lett.* **61**, 1198–1201.
- FUNFSCHILLING, D., BROWN, E., NIKOLAENKO, A. & AHLERS, G. 2005 Heat transport by turbulent Rayleigh-Bénard convection in cylindrical cells with aspect ratio one and larger. *J. Fluid Mech.* **536**, 145–154.
- FURUKAWA, A. & ONUKI, A. 2002 Convective heat transport in compressible fluids. *Phys. Rev. E* **66**, 016302.
- GITTERMAN, M. 1978 Hydrodynamics of fluids near a critical point. *Rev. Mod. Phys.* **50**, 85–107.
- GITTERMAN, M. & STEINBERG, V. 1971 Criteria of occurrence of free convection in a compressible viscous heat-conducting fluid. *J. Appl. Math. Mech. (USSR)* **34**, 305–311.
- GROSSMANN, S. & LOHSE, D. 2000 Scaling in thermal convection: A unifying view. *J. Fluid Mech.* **407**, 27–56.
- GROSSMANN, S. & LOHSE, D. 2001 Thermal convection for large Prandtl number. *Phys. Rev. Lett.* **86**, 3316–3319.
- GROSSMANN, S. & LOHSE, D. 2002 Prandtl and Rayleigh number dependence of the Reynolds number in turbulent thermal convection. *Phys. Rev. E* **66**, 016305.
- GROSSMANN, S. & LOHSE, D. 2004 Fluctuations in turbulent Rayleigh-Bénard convection: The role of plumes. *Phys. Fluids* **16**, 4462–4472.
- HOARD, C., ROBERTSON, C. & ACRIVOS, A. 1970 Experiments on the cellular structure in Bénard convection. *Int. J. Heat Mass Transfer* **13**, 849–856.
- KOGAN, A. & MEYER, H. 2001 Heat transfer and convection onset in a compressible fluid: ³He near the critical point. *Phys. Rev. E* **63**, 056310:1–15.

- KRAICHNAN, R. H. 1962 Turbulent thermal convection at arbitrary Prandtl number. *Phys. Fluids* **5**, 1374–1389.
- LANDAU, L. D. & LIFSHITZ, E. M. 1987 *Fluid Mechanics*. Oxford: Pergamon Press.
- MEKSYN, D. 1961 *New Methods in Laminar Boundary Layer Theory*. Oxford: Pergamon Press.
- NIEMELA, J., SKREBEK, L., SREENIVASAN, K. R. & DONNELLY, R. J. 2001 The wind in confined thermal turbulence. *J. Fluid Mech.* **449**, 169–178.
- NIEMELA, J., SKREBEK, L., SREENIVASAN, K. R. & DONNELLY, R. 2000 Turbulent convection at very high Rayleigh numbers. *Nature* **404**, 837–840.
- NIEMELA, J. & SREENIVASAN, K. R. 2003 Confined turbulent convection. *J. Fluid Mech.* **481**, 355–384.
- NIKOLAENKO, A., BROWN, E., FUNFSCHILLING, D. & AHLERS, G. 2005 Heat transport by turbulent Rayleigh-Bénard convection in cylindrical cells with aspect ratio one and less. *J. Fluid Mech.* **523**, 251–260.
- OBERBECK, A. 1879 Über die Wärmeleitung der Flüssigkeiten bei Berücksichtigung der Strömungen infolge von Temperaturdifferenzen. *Ann. Phys. Chem.* **7**, 271–292.
- OH, J., ORTIZ DE ZÁRATE, J. M., SENGERS, J. V. & AHLERS, G. 2004 Dynamics of fluctuations in a fluid below the onset of Rayleigh-Bénard convection. *Phys. Rev. E* **69**, 021106.
- PAMPALONI, E., PEREZ-GARCIA, C., ALBAVETTI, L. & CILIBERTO, S. 1992 Transition from hexagons to rolls in convection in fluids under non-Boussinesq conditions. *J. Fluid Mech.* **234**, 393–416.
- PLAPP, J. E. 1957 Laminar free convection with variable fluid properties. PhD thesis, Caltech, available at <http://resolver.caltech.edu/CaltechETD:etd-09142004-153230>.
- POHLHAUSEN, E. 1921 Der Wärmeaustausch zwischen Festkörpern und Flüssigkeiten mit kleiner Reibung und kleiner Wärmeleitung. *Z. Angew. Math. Mech.* **1**, 115–121.
- PRANDTL, L. 1905 *Über Flüssigkeitsbewegung bei sehr kleiner Reibung*, pp. 484–491. Leipzig: Teubner.
- PRESS, W., TEUKOLSKY, S., VETTERLING, W. & FLANNERY, B. 1986 *Numerical Recipes*. Cambridge: Cambridge University Press.
- QIU, X. L. & TONG, P. 2001a Large scale velocity structures in turbulent thermal convection. *Phys. Rev. E* **64**, 036304.
- QIU, X. L. & TONG, P. 2001b Onset of coherent oscillations in turbulent Rayleigh-Bénard convection. *Phys. Rev. Lett.* **87**, 094501.
- ROCHE, P. E., CASTAING, B., CHABAUD, B. & HEBRAL, B. 2001 Observation of the 1/2 power law in Rayleigh-Bénard convection. *Phys. Rev. E* **63**, 045303.
- ROCHE, P. E., CASTAING, B., CHABAUD, B. & HEBRAL, B. 2002 Prandtl and Rayleigh numbers dependences in Rayleigh-Bénard convection. *Europhys. Lett.* **58**, 693–698.
- SCHLICHTING, H. & GERSTEN, K. 2000 *Boundary layer theory*, 8th edn. Berlin: Springer Verlag.
- SHRAIMAN, B. I. & SIGGIA, E. D. 1990 Heat transport in high-Rayleigh number convection. *Phys. Rev. A* **42**, 3650–3653.
- SUN, C., REN, L. Y., SONG, H., AND XIA, K. Q. 2005 Heat transport by turbulent Rayleigh-Bénard convection in 1 m diameter cylindrical cells of widely varying aspect ratio. *J. Fluid Mech.* **542**, 165–174.
- VERZICCO, R. 2002 Sidewall finite conductivity effects in confined turbulent thermal convection. *J. Fluid Mech.* **473**, 201–210.
- VERZICCO, R. 2004 Effect of non-perfect thermal sources in turbulent thermal convection. *Phys. Fluids* **16**, 1965–1979.
- WALDEN, R. W. & AHLERS, G. 1981 Non-Boussinesq and penetrative convection in a cylindrical cell. *J. Fluid Mech.* **109**, 89–114.
- WALL, D. P. & WILSON, S. K. 1997 The linear stability of flat-plate boundary-layer flow of fluid with temperature-dependent viscosity. *Phys. Fluids* **9**, 2885–2898.
- WU, X. Z. & LIBCHABER, A. 1991 Non-Boussinesq effects in free thermal convection. *Phys. Rev. A* **43**, 2833–2839.
- XU, X., BAJAJ, K. M. S. & AHLERS, G. 2000 Heat transport in turbulent Rayleigh-Bénard convection. *Phys. Rev. Lett.* **84**, 4357–4360.
- ZHANG, J., CHILDRESS, S. & LIBCHABER, A. 1997 Non-Boussinesq effect: Thermal convection with broken symmetry. *Phys. Fluids* **9**, 1034–1042.